Understanding Arctic Sea Ice Thickness Predictability by a Markov Model

YUNHE WANG,[a,d] XIAOJUN YUAN,[b] HAIBO BI,[c,d] YIBIN REN,[a,d] YU LIANG,[c,e] CUIHUA LI,[b] AND XIAOFENG LI[a,d]

[a] *CAS Key Laboratory of Ocean Circulation and Waves, Institute of Oceanology, Chinese Academy of Sciences, Qingdao, China*
[b] *Lamont-Doherty Earth Observatory, Columbia University, Palisades, New York*
[c] *CAS Key Laboratory of Marine Geology and Environment, Institute of Oceanology, Chinese Academy of Sciences, Qingdao, China*
[d] *Center for Ocean Mega-Science, Chinese Academy of Sciences, Qingdao, China*
[e] *University of Chinese Academy of Sciences, Beijing, China*

(Manuscript received 12 July 2022, in final form 10 March 2023, accepted 24 March 2023)

ABSTRACT: The Arctic sea ice decline and associated change in maritime accessibility have created a pressing need for sea ice thickness (SIT) predictions. This study developed a linear Markov model for the seasonal prediction of model-assimilated SIT. It tested the performance of physically relevant predictors by a series of sensitivity tests. As measured by the anomaly correlation coefficient (ACC) and root-mean-square error (RMSE), the SIT prediction skill was evaluated in different Arctic regions and across all seasons. The results show that SIT prediction has better skill in the cold season than in the warm season. The model performs best in the Arctic basin up to 12 months in advance with ACCs of 0.7–0.8. Linear trend contributions to model skill increase with lead months. Although monthly SIT trends contribute largely to the model skill, the model remains skillful up to 2-month leads with ACCs of 0.6 for detrended SIT predictions in many Arctic regions. In addition, the Markov model's skill generally outperforms an anomaly persistence forecast even after all trends were removed. It also shows that, apart from SIT itself, upper-ocean heat content (OHC) generally contributes more to SIT prediction skill than other variables. Sea ice concentration (SIC) is a relatively less sensitive predictor for SIT prediction skill than OHC. Moreover, the Markov model can capture the melt-to-growth season reemergence of SIT predictability and does not show a spring predictability barrier, which has previously been observed in regional dynamical model forecasts of September sea ice area, suggesting that the Markov model is an effective tool for SIT seasonal predictions.

KEYWORDS: Arctic; Sea ice; Climate prediction; Ice thickness

1. Introduction

Associated with internal climate variability and anthropogenic greenhouse gas emissions (England et al. 2021), Arctic near-surface air temperatures continue to increase at 3–4 times the rate of the global average (Ballinger et al. 2021; Chylek et al. 2022), a phenomenon known as "Arctic amplification," caused by various positive feedbacks (Screen and Simmonds 2010; Pithan and Mauritsen 2014). Meanwhile, Arctic sea ice's properties have dramatically changed during recent decades (Notz and Stroeve 2016; Wang et al. 2019a; Cai et al. 2021; X. Wang et al. 2022). The pan-Arctic sea ice extent (SIE) has shown a consistent decline for all months since late 1978 (Liu et al. 2019). Sea ice thickness (SIT) has been thinning (Kwok 2018; Meier et al. 2021), with thicker multiyear sea ice being replaced by thinner seasonal sea ice (Tschudi et al. 2016). Sea ice volume (SIV) was at a record low in April 2021 since 2010 (Meier et al. 2021). Climate simulations project the Arctic to be ice-free in the summer by 2050 (Notz and SIMIP Community 2020). Other studies put this date as early as the 2030s (Guarino et al. 2020).

Sea ice acts as a crucial component of the climate system by regulating heat, moisture, and momentum flux exchanges between the atmosphere and the polar oceans (Peterson et al. 2017; Smith et al. 2017). Such dramatic thinning of Arctic sea ice has profound local and remote consequences. It contributes to the penetration of solar energy into the ocean (Katlein et al. 2019), polar temperature amplification (Kim et al. 2016; Screen and Francis 2016; Labe et al. 2018), and a nonnegligible influence on the large-scale dynamic circulation over the Arctic Ocean and northern Eurasia (Labe et al. 2018). Sea ice loss also possibly contributed to a weakening of the midlatitude jet (Francis and Vavrus 2012) and increased frequency of extreme Northern Hemisphere winters by weakening the stratospheric polar vortex (Meleshko et al. 2018; Cohen et al. 2020), but this point remains controversial (Blackport et al. 2019). The thinning sea ice is also associated with freshwater transport to the south and modulates sea surface salinity, weakening the Atlantic meridional overturning circulation (AMOC) (Yang et al. 2016; Sévellec et al. 2017; Suo et al. 2017).

Beyond influencing the climate system, the continued dramatic decline in Arctic sea ice has changed maritime accessibility. This has gained the attention of various industry and community groups ranging from Arctic commercial shipping (Chen et al. 2021; Zhou et al. 2021), natural resource extraction (Semenova 2022), fishery activities (Fauchald et al. 2021), and indigenous communities who rely on sea ice for travel

Denotes content that is immediately available upon publication as open access.

Supplemental information related to this paper is available at the Journals Online website: https://doi.org/10.1175/JCLI-D-22-0525.s1.

Corresponding authors: Xiaojun Yuan, xyuan@ldeo.columbia.edu; Xiaofeng Li, lixf@qdio.ac.cn

DOI: 10.1175/JCLI-D-22-0525.1

and subsistence (Segal et al. 2020). For example, the Northern Sea Route extends along the northern coast of Eurasia from Iceland to the Bering Strait, which shortens the transit distance by approximately 5000 nautical miles (n mi; 1 n mi = 1.852 km) relative to the southern routes through the Suez Canal (Lee and Song 2014). Substantial reductions in distance can result in large cost savings due to reduced fuel consumption. Therefore, societal and economic perspectives have led to increasing efforts in Arctic sea ice prediction in recent decades (Liu et al. 2019).

Substantial effort has gone toward developing prediction approaches of sea ice properties varying from dynamical models to statistical models and deep learning. Dynamical models numerically solve equations that govern climate system dynamics and thermodynamics using ice–ocean–atmosphere or ice–ocean conditions to initialize the models for each season (Msadek et al. 2014; Blanchard-Wrigglesworth et al. 2015; Peterson et al. 2015; Bushuk et al. 2020; Dai et al. 2020; Bushuk et al. 2021; Lee et al. 2022; Yang et al. 2022). Unfortunately, dynamical models are imperfect, and modeling challenges still exist in many parameterization processes, including ice thickness distribution, wave–ice interaction, rheology, melt ponding, land-fast ice, and floe size distribution (Leppäranta et al. 2020). Past summaries of submissions to the Sea Ice Outlook, a community network activity led by the Sea Ice Prediction Network Phase 2 (SIPN2) Project Team, Bhatt et al. (2022) have shown that generally dynamical models do not significantly outperform their statistical model counterparts. In fact, physics-based dynamical models can successfully forecast sea ice properties several weeks ahead, and they struggle to outperform simple statistical forecasts at longer lead times (Guemas et al. 2016a; Wayand et al. 2019). This leaves a window open to explore statistical models.

Statistical models can be constructed from relationships among sea ice variables and oceanic and atmospheric conditions. Recently, statistical methods have been used to provide sea ice field [sea ice concentration (SIC) and SIE] predictions using numerous techniques such as the linear Markov model (Yuan et al. 2016; Wang et al. 2022a), vector autoregressive model (L. Wang et al. 2016, 2019), Bayesian logistic regression (Horvath et al. 2020), multiple linear regression model (Ionita et al. 2019), and a combination of complex networks and Gaussian process regression model (Gregory et al. 2020). Statistical models have, in some cases, shown promise in exploiting sources of predictability at a 4-month or longer lead time (Lindsay et al. 2008; Stroeve et al. 2016; Yuan et al. 2016; Ionita et al. 2019). Wang et al. (2022a) showed that a linear Markov model has skillful SIC predictions up to 7-month lead times in the Pacific–Arctic sector.

In addition, deep learning (DL) is a field of study in computer science and a type of artificial intelligence that provides the capability to learn representations of data or to predict data using computational methods with multiple layers (Chi and Kim 2017; Kim et al. 2020; Andersson et al. 2021; Liu et al. 2021). DL has been successfully applied to sea ice forecasting and achieved remarkable results at the synoptic scale (Ren et al. 2022). However, DL requires large volumes of datasets for the training process and enough validation data for statistical significance tests. The observed sea ice time series of 43 years can hardly meet the "big data" requirement at a seasonal time scale (Liu et al. 2021).

Although numerous studies have documented predicting SIC, SIE, and sea ice area (SIA), few have investigated Arctic SIT prediction. For example, Ponsoni et al. (2020) evaluated the statistical predictability of the Arctic SIV. They found that SIT has relatively large spatial autocorrelation and is the best predictor apart from the SIV itself. Gao et al. (2022) proposed a statistical spatiotemporal two-stage model for SIT and used it to generate probabilistic forecasts up to 3-month leads. Furthermore, SIT predictions have potential value for various industry and community groups. For example, operation of icebreakers requires knowledge of SIT to ensure safety and establish the viability of transit to northern ports (Huntington et al. 2015). Many engineering problems require an estimate of ice thickness. SIT also allows us to predict ice mass budgets.

Unfortunately, unlike SIC and SIE, which have been continuously observed by satellites for more than four decades, long records of SIT observations are lacking (Lindsay and Schweiger 2015; Dawson et al. 2022; Fiedler et al. 2022). Although altimeter-based satellite measurements have begun to fill this gap and machine learning can now estimate summer SIT (Landy et al. 2022), these time series are not long enough to support statistical modeling. Nevertheless, the Pan-Arctic Ice Ocean Modeling and Assimilation System (PIOMAS) provides a spatially and temporally complete simulation of Arctic SIT over the satellite era from 1979 to the present (Zhang and Rothrock 2003). PIOMAS compares reasonably well to available satellite, aircraft, and in situ SIT measurements (Schweiger et al. 2011; Laxon et al. 2013; Ponsoni et al. 2019) and has become a reference dataset in Arctic climate studies (Mu et al. 2018; Shamshiri et al. 2022).

In this study, we aim to develop a linear Markov model configured for the PIOMAS SIT seasonal prediction and test the performance of physically relevant predictors, including SIC, atmospheric, and oceanic variables in SIT prediction. We also check whether Arctic SIT prediction shows a spring predictability barrier, which has previously been observed in regional dynamical model forecasts of sea ice area (Bonan et al. 2019; Bushuk et al. 2020) and understand unique SIT driving processes in different seasons. We follow the framework of the Markov model developed by Wang et al. (2022a), which consists of four modules with seasonal dependent variables and isolates the dominant processes for each targeted season. SIT predictability is assessed at grid points and over all seasons and subsequently compared with the SIT anomaly persistence.

2. Data and methods

a. Potential predictors

This section identifies potential predictors as input into the Markov model for SIT seasonal prediction. Generally, sea ice is closely coupled with the ocean and atmosphere. Sea ice predictability is mainly provided by the intrinsic memory of sea

ice and its related variables. Thus, accurate definition of the state of the Arctic climate is the key to sea ice prediction. Wang et al. (2022a) showed that the ocean heat content (OHC) and SIT provide significant skill for Arctic SIC seasonal prediction. Moreover, the accurate definition of the state of the Arctic climate requires not only SIT and OHC but also other variables that influence sea ice through dynamic or thermodynamic processes (Guemas et al. 2016a; Yuan et al. 2016; Wang et al. 2019b; Ponsoni et al. 2020; Wang et al. 2022a,b). Here, we choose to define the ocean–ice–atmosphere coupled Arctic climate system with nine variables: SIT, SIC, OHC in the upper 300 m, sea surface temperature (SST), surface air temperature (SAT), 850-hPa geopotential height (GPH), 850-hPa wind vector, surface net radiative flux (SNRF), and surface net turbulent heat flux (SNTF).

Monthly SITs are from the PIOMAS model product, which is a coupled ocean–ice model that assimilates daily SIC, sea ice motion (SIM), and SST satellite products (Zhang and Rothrock 2003). PIOMAS couples the Parallel Ocean Program (POP) ocean model with a 12-category thickness and enthalpy distribution (TED) sea ice model and an assimilation system. The TED sea ice model originates from the Thorndike thickness distribution theory (Thorndike et al. 1975) and was enhanced by the enthalpy distribution theory (Zhang and Rothrock 2001). The system is forced by National Centers for Environmental Prediction–National Center for Atmospheric Research (NCEP–NCAR) reanalysis, including 2-m SAT, 10-m surface winds, cloud fraction, downwelling longwave radiation, precipitation, etc. Compared with 14 other reanalyses, Ponsoni et al. (2019) showed that PIOMAS SIT is in the best agreement with the observations that the root-mean-square error (RMSE) and anomaly correlation coefficient (ACC) between the two datasets are 0.7 m and 0.66, respectively. However, PIOMAS appears to overestimate SIT in the thin-ice area of the Beaufort Sea and underestimate SIT around the north coast of Canadian Arctic Archipelago (CAA) and Greenland compared to IceBridge (X. Wang et al. 2016). Uncertainties in PIOMAS SIT are mainly from the model forcing, physics, and parameterizations (Chylek et al. 2022). PIOMAS provides estimates of multiple ocean and ice variables such as SIT, SIM, surface temperature, and upper-ocean salinity, and covers the period from 1978 onward when satellite ice concentration data are available for assimilation.

The CS2SMOS, merged *CryoSat-2*/SMOS satellite SIT data using an optimal interpolation scheme (Ricker et al. 2017), are used to verify the PIOMAS SIT products. Actually, SMOS satellite can observe thin seasonal sea ice, and *CryoSat-2* is designed to detect thicker multiyear sea ice. Thus, CS2SMOS merges these satellite observations and provides a more complete and accurate picture of the state of changing Arctic SIT. Compared to airborne SIT data, CS2SMOS shows an improvement over *CryoSat-2* in the thin ice regimes and has a low bias in the mixed seasonal and multiyear ice regimes. The CS2SMOS SIT covers the wintertime (October–April) from November 2010 onward.

Monthly SICs, on an equal-area polar stereographic projection with a spatial resolution of 25 km, are obtained from the National Snow and Ice Data Center (NSIDC) (Comiso 2017). The dataset was derived from passive microwave radiometers, including Scanning Multichannel Microwave Radiometer (SMMR) on *Nimbus-7* satellite, Special Sensor Microwave Imager (SSM/I) on satellites of the Defense Meteorological Satellite Program (DMSP), and the Special Sensor Microwave Imager/Sounder (SSMIS) aboard DMSP-*F17*. The dataset was generated using the bootstrap algorithm with daily varying tie points.

The OHC data, from the global ocean–sea ice reanalysis (ORAS5: Ocean Reanalysis System 5), were developed by the European Centre for Medium-Range Weather Forecasts (ECMWF) OCEAN5 ocean analysis–reanalysis system and cover the period from 1979 onward (Zuo et al. 2019). SST and atmospheric variables are obtained from the latest ECMWF reanalysis version 5 (ERA5) with a spatial resolution of 1° (Hersbach et al. 2020). ERA5 is produced using the version of ECMWF's Integrated Forecast System (IFS), CY41R2, based on a hybrid incremental 4D-Var system. These variables are used to define the state of the atmosphere and ocean coupled system for Markov model development.

b. *Markov model*

Here the Markov model follows the model framework used in an earlier study (Wang et al. 2022a), which was an improved version of Yuan et al. (2016). In addition to adding OHC and SIT as model predictors, the updated Markov model also consists of four seasonal modules with different sets of predictors instead of being developed with one set of variables for all seasons. Seasons are defined as follows: winter (December–February), spring (March–May), summer (June–August), and autumn (September–November). The improved skill of the new model is mainly attributed to the fact that the multimonth persistence of OHC and SIT anomalies provides a crucial source of sea ice predictability and four seasonal modules enable the model to accommodate seasonally varying driving processes.

The updated Markov model is also constructed in the multivariate empirical orthogonal functions (MEOF) space. The base functions of the model's spatial dependence consist of the MEOF eigenvectors calculated from these nine variables, while the temporal evolution of the model is a Markov process. Transition functions are accordingly determined by the corresponding principal components (PCs). In other words, the Markov model for sea ice prediction is built on multivariate models, which can capture the covariability in the ocean–ice–atmosphere coupled system instead of linearly regressing on individual predictors. To reduce the model space and filter out unpredictable small-scale features, we use only a subset of leading MEOF modes. Therefore, the dominance of leading modes in the climate system and the model's ability to pick up these modes are the keys to the success of the Markov model.

We preselect the SIT, SIC, OHC, SST, SAT, 850-hPa GPH, 850-hPa wind vector, SNRF, and SNTF to define the coupled Arctic surface climate system. To reduce model dimensions, we remove mostly open-water and land grid cells from the SIC and SIT fields. The mostly open-water area is defined by the cells where SIC $\leq 15\%$ occurred more than 96% of the total all-season time series. We gridded all variable fields onto

the native NSIDC 25-km polar stereographic grid and created anomalies from 1979 to 2020 by subtracting climatologies from monthly time series and keeping trends. Each anomaly variable field is normalized via being divided by the standard deviation of the time series at each grid cell. To emphasize the SIT variability signal in the model construction, we weight the normalized SIT anomalies by 2 and keep the other variables unchanged. Those normalized variable fields are then stacked into a single matrix $\mathbf{V}$ (n, m), where n is the number of grid cells of all fields (6823 for each field) and m is the length of the time series (504). We decompose $\mathbf{V}$ into eigenvectors $\mathbf{E}$ and their corresponding principal components (PCs, time series) $\mathbf{P}$:

$$\mathbf{V} = \mathbf{E}\mathbf{P}^{\mathrm{T}}, \tag{1}$$

where the columns of $\mathbf{E}$ are orthogonal and the columns of $\mathbf{P}$ are orthonormal; the superscript T denotes matrix transpose. In this work, Eq. (1) is truncated to a subset of leading modes. The truncation is determined by how skill and error depends on the number of EOFs retained (see section 3 and Fig. 2). The Markov model is computed using the single-step correlation matrix, which is a transition matrix $\mathbf{A}$ satisfying the following linear relation:

$$\mathbf{P}_{i+1} = \mathbf{A}\mathbf{P}_i + e_i, \tag{2}$$

where i is the ith calendar month and e_i is the error in the model fit. Transition matrix $\mathbf{A}$ is computed by multiplying Eq. (2) with $\mathbf{P}_i^{\mathrm{T}}$

$$\mathbf{P}_{i+1}\mathbf{P}_i^{\mathrm{T}} = \mathbf{A}\mathbf{P}_i\mathbf{P}_i^{\mathrm{T}} + e_i\mathbf{P}_i^{\mathrm{T}}. \tag{3}$$

For the best model fit, e_i and $\mathbf{P}_i^{\mathrm{T}}$ should have no correlation. Thus,

$$\mathbf{A} = (\mathbf{P}_{i\,i+1}^{\mathrm{T}}\mathbf{P}_i^{\mathrm{T}})(\mathbf{P}_i\mathbf{P}_i^{\mathrm{T}})^{-1}. \tag{4}$$

Transition matrix $\mathbf{A}$ is constructed to be seasonally dependent because of the strong seasonality of SIT and related variables. Thus, Eq. (4) is applied to 12 subsets of PCs to obtain corresponding transition matrices for each of the 12 calendar months. It is worth mentioning that the term "target month" refers to the month that is being predicted throughout the manuscript, and "lead month" refers to the number of months prior to the target month that the forecast was initialized.

Then, Arctic SIT seasonal prediction can be carried out through the following five steps:

1) We create 12 variable combinations representing different aspects of climate conditions to examine which variable or combination of variables provides the highest SIT prediction skill.
2) The PCs corresponding to each combination of variables are computed by the MEOF Eq. (1) with different truncations of leading modes.
3) Transition matrices $\mathbf{A}$ corresponding to calendar months are calculated by Eq. (4).
4) The predictions of the PCs are made by Eq. (2) one lead month at a time, applying the corresponding transition matrices.
5) The predicted PCs are combined with the respective eigenvectors to generate SIT anomaly prediction for each variable combination.

The prediction skill is measured by the ACC, percentage of grid points with significant ACC (PGS), and RMSE between PIOMAS SITs and predictions. We train the Markov model using a cross-validation scheme (Barnston and Ropelewski 1992) that builds a model with a 1-yr moving window of data removal and then use this window of data to evaluate the model performance. Specifically, we remove one year of time series from a PC and use the rest of the PC to calculate the transition matrix. Then we make a 12-month prediction of PC for that year. We repeat the procedure for each year of PCs and obtain the cross-validated predicted PCs from 1980 to 2020. Such a cross-validated experimental design reduces artificial skill without compromising the length of the time series. The superior model configuration for each season thus can be identified by testing the Markov model with different variable combinations and different truncation of modes in the cross-validated model experiments. The complete SIT anomaly predictions can then be generated by combining subpredictions made by the optimal model in each season. The predicted SIT anomalies are divided by a weight value of 2, multiplied by the standard deviation, and the climatology is added to generate the complete SIT predictions.

To assess the ability of the Markov model to predict regional SIT, the Arctic is separated into 12 subregions (Fig. 1). The regional domains are chosen following the NSIDC definitions. In addition, the SIT shows an extensive thinning throughout the Arctic Ocean basin, especially in the East Siberian Sea, and a narrow band along the Canadian Arctic Archipelago (CAA) and Greenland (Fig. S1 in the online supplemental material). The variability in SIT measured by the standard deviation of anomaly is also high in these regions with large linear trends. As the trends are essential parts of the total variability, we retain the trends in SIT anomalies while building the Markov model and also conduct a postprediction evaluation of the impact of trends on the model skill.

3. Prediction experiments and evaluation of predictors

To construct an optimal model for each season, we first examined the prediction skill of models with different initial climate conditions to determine which variable combinations and number of modes should be retained in building a Markov model. As the modes are sorted based on the explained variance in the MEOF analysis, using too few leading modes in the model will miss some predictable signals, and too many may lead to overfitting and contaminate the model with unpredictable small-scale features. For this practical issue, we tested the prediction skill and sensitivity of the model through a series of cross-validated model experiments with different variables and numbers of leading modes. The variable combinations are listed in Table 1. Models with V2–V7 and V9–V11

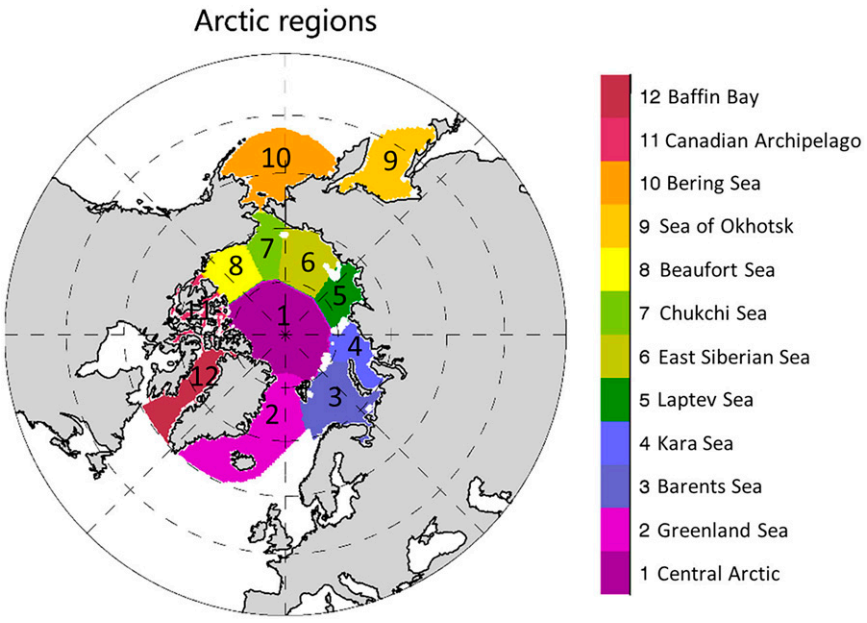

FIG. 1. Arctic regions used in this study.

are weighted toward thermodynamic processes, while V8 and V12 represent the integration of thermodynamic and dynamic processes. In addition, we first evaluated the contribution of each predictor to the model skill by using V1–V8 and further combined better predictors into more-variable combinations (V9–V11) to determine the optimal variable combination in the Markov model. V1 and V12 were used as the control combinations in the model experiment.

The cross-validation scheme was carried out for the PCs decomposed from each variable combination to make predictions at 1–12-month leads. The PGS and mean RMSE for each lead time in each season were calculated to test the model's sensitivity. We retained up to 30 modes in the model to avoid missing fundamental predictable signals and then determined the best model configuration according to model skill. We averaged the model prediction skill at all lead times for each season, and the results are shown in Fig. 2. In general, models with high ACC have a smaller RMSE. Figure 2 shows that the predictive skill decreases steeply and RMSE increases after 26 modes for all seasons, especially in summer and autumn, implying that the modes beyond mode 26 mainly represent unpredictable small-scale features. In addition, the model with fewer than 3 modes misses many predictable signals. Similar to the SIC prediction, the SIT prediction model also needs more modes in winter and spring than in summer and autumn, which is likely due to the greater regional SIT variability and relatively weaker trends in the cold season. In contrast, the model skill is better during the cold season, contrary to the Markov model for SIC prediction (Wang et al. 2022a).

The contribution of different variables to SIT prediction skill in each season was also assessed. Undoubtedly, the model skill comes primarily from SIT itself. The model based on V1 (SIT only) has PGS scores above 85% in the cold season and above 80% in the warm season. It also has a relatively low RMSE without additional information (Fig. 2). Adding other oceanic and atmospheric variables, especially the ocean information, the Markov model can further improve the prediction skill because it can capture the covariability in the ocean–ice–atmosphere coupled system. However, SIC cannot

TABLE 1. Variable combinations in cross-validated experiments. V1 represents the no. 1 variable combination. A √ denotes a variable included in the corresponding combination.

	V1	V2	V3	V4	V5	V6	V7	V8	V9	V10	V11	V12
SIT	√	√	√	√	√	√	√	√	√	√	√	√
SIC		√										√
OHC			√						√	√	√	√
SST				√					√		√	√
SAT					√				√		√	√
SNTF						√				√	√	√
SNRF							√			√	√	√
GPH, *U*, *V*								√				√

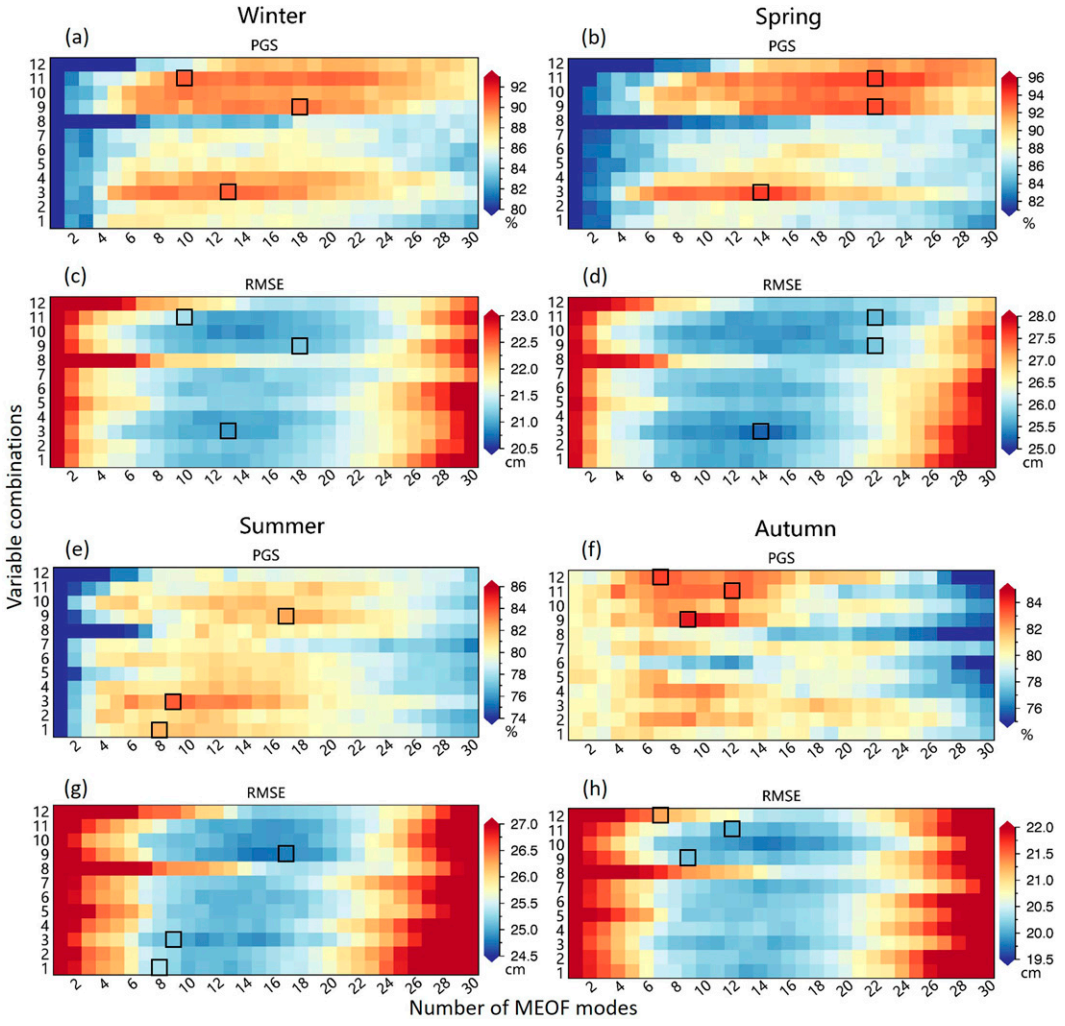

FIG. 2. Mean PGS and RMSE between SIT predictions and PIOMAS data in each season. (a) Mean PGS for winter target months is obtained by averaging prediction skill at 1–12-month leads. The *x* axis is the number of MEOF modes, and the *y* axis is variable combinations corresponding to Table 1. (b),(e),(f) As in (a), but for spring, summer, and autumn target months, respectively. (c),(d),(g),(h) As in (a), (b), (e), and (f), but for RMSE. PGS denotes percentage of grid points with significant ACC and helps us to determine the model configuration.

provide much skill for SIT prediction, especially during the cold season, because the Arctic Basin is mostly covered by sea ice with near 100% concentration in the cold season with little variability. At the same time, there is still significant variability in the SIT. Thus, SIC does not contribute significantly to SIT predictability.

OHC generally contributes more to the SIT prediction skill than other variables. At the same time, the model with SST is more prominent in autumn (Fig. 2), suggesting that the ocean provides a considerable source of memory for SIT prediction skill and plays a crucial role in SIT variability. The results are consistent with previous studies that the SST memory of spring climate anomaly allows sea ice anomaly to reemerge in the following ice growth season (Guemas et al. 2016b; Bushuk et al. 2017; Dai et al. 2020; Lenetsky et al. 2021). In the cold season, the Arctic Ocean is almost covered by sea ice resulting in the SSTs being almost constant with no variability, which does not correspond with the SIT variability. In the warm season, especially in autumn, sea ice coverage is minimal. Therefore, the SST variability is the most significant over the year, which could substantially contribute to the SIT prediction skill. Compared with SST records, the OHC record shows a larger signal-to-noise ratio (Cheng et al. 2018), which is beneficial for EOF to capture the leading variability signal of OHC. The coupled relationship between OHC and SIT can be captured by MEOF analysis, showing that negative OHC anomalies correspond to positive SIT anomalies and vice versa. However, minor inconsistencies occur in some modes and regions (Fig. S3). In addition, the explained variance of the leading MEOF modes of SIT and OHC is greater than that of SIT, GPH, and winds (Fig. S4). This reflects that the ocean can provide more prediction skill than the atmosphere on a seasonal

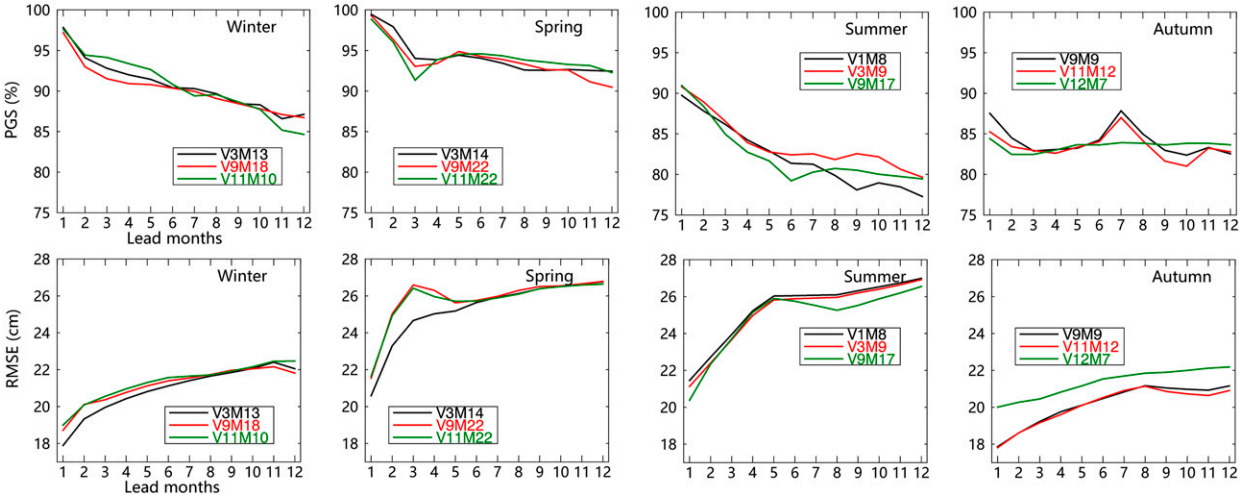

FIG. 3. Prediction skill for preliminary selection of superior models in each season. (a)–(d) Prediction skill measured by mean PGS for each target season. (e)–(h) As in (a)–(d), but for RMSE. V3M13 marked in legend represents the model constructed by the number 3 variable combination with up to 13 leading modes.

scale. Therefore, the OHC plays a crucial role in sea ice variability for all seasons and provides a significant memory source for the SIT prediction skill.

In addition, the prediction skills provided by SAT, turbulent heat flux, and radiative heat flux are also not as significant as those provided by OHC. The dynamic climatic conditions defined by GPH and winds even have a negative impact on SIT prediction by the Markov model, which we will further discuss in section 6.

Based on the model skill measured by PGS and RMSE, we primarily selected three superior model configurations marked by black boxes in Fig. 2 for each season. To further determine which model configuration makes the best prediction in each season, we spatially averaged the prediction skill for 1–12-month leads (Fig. 3). The prediction skill of those superior models has similar magnitudes and variabilities in winter, while large differences occur in autumn. It also shows that the model skill rapidly decreases between 1 and 3 lead months in spring. In other words, the model does not perform well in SIT predictions during spring using the previous winter's initial conditions. Moreover, the model skill in autumn increases steeply at the 7-month lead, suggesting that the model performs better in autumn SIT prediction using spring initial data. This correlation feature refers to melt-season SIT anomalies to recur the following ice growth season. It could be related to the SST reemergence that spring SST anomalies are stored beneath the summer mixed layer and reemerge to the surface when the mixed layer deepens the following autumn (Blanchard-Wrigglesworth et al. 2011; Bushuk and Giannakis 2017). Therefore, the oceanic memory could induce sea-ice anomalies during the growth season and partially contributes to long-lead SIT predictability.

To avoid possible overfitting, we chose the configuration with the minimum number of variables and modes from these superior models with roughly the same level of skill. Therefore, we chose V3M13 and V3M14 as the best models for winter and spring, respectively, since they show the lowest RMSE and fewer variables and modes. We chose V3M9 for summer since it shows the highest PGS. For autumn, we chose V9M9 because it performs best at 1–8 lead months, although V12M7 dominates PGS beyond the 9-month lead.

4. Prediction skill assessment

The SIT predictions made by the model built above were evaluated at each grid cell and for all seasons using the cross-validated model skill measured by ACC and RMSE. The model skill is presented at 3, 6, 9, and 12 lead months (Fig. 4). Overall, the model has higher prediction skill for cold seasons than for warm seasons, which is contrary to Arctic SIC prediction (Wang et al. 2022a). The skill of SIT predictions also does not show regional differences between the Atlantic and Pacific sectors, as shown by skill features of SIC predictions. The skill in the central Arctic basin is highest in winter, and the skill in the peripheral seas is highest in spring. The summer prediction skill shows a similar pattern as the autumn skill but with a roughly 0.1 higher ACC. In addition, the model skill decreases gradually with an increase in lead months, but it is still significant even at 12-month leads for all seasons in the Arctic basin. Spatially, high forecast skill is concentrated in the central Arctic basin, where the SIC predictability is very low. The Bering Sea and the Sea of Okhotsk show moderate prediction skills during cold seasons, whereas the skills disappear in warm seasons since sea ice completely melts in those areas. The main controlling factors of the spatial feature in the model skill are further discussed in section 6.

RMSEs are consistent with ACC: low RMSEs correspond to high correlations, and vice versa, although minor inconsistencies occur in some regions (Fig. 5). The SIT prediction errors are most significant along the coastlines of the Arctic Ocean and smallest in the interior Arctic and the peripheral

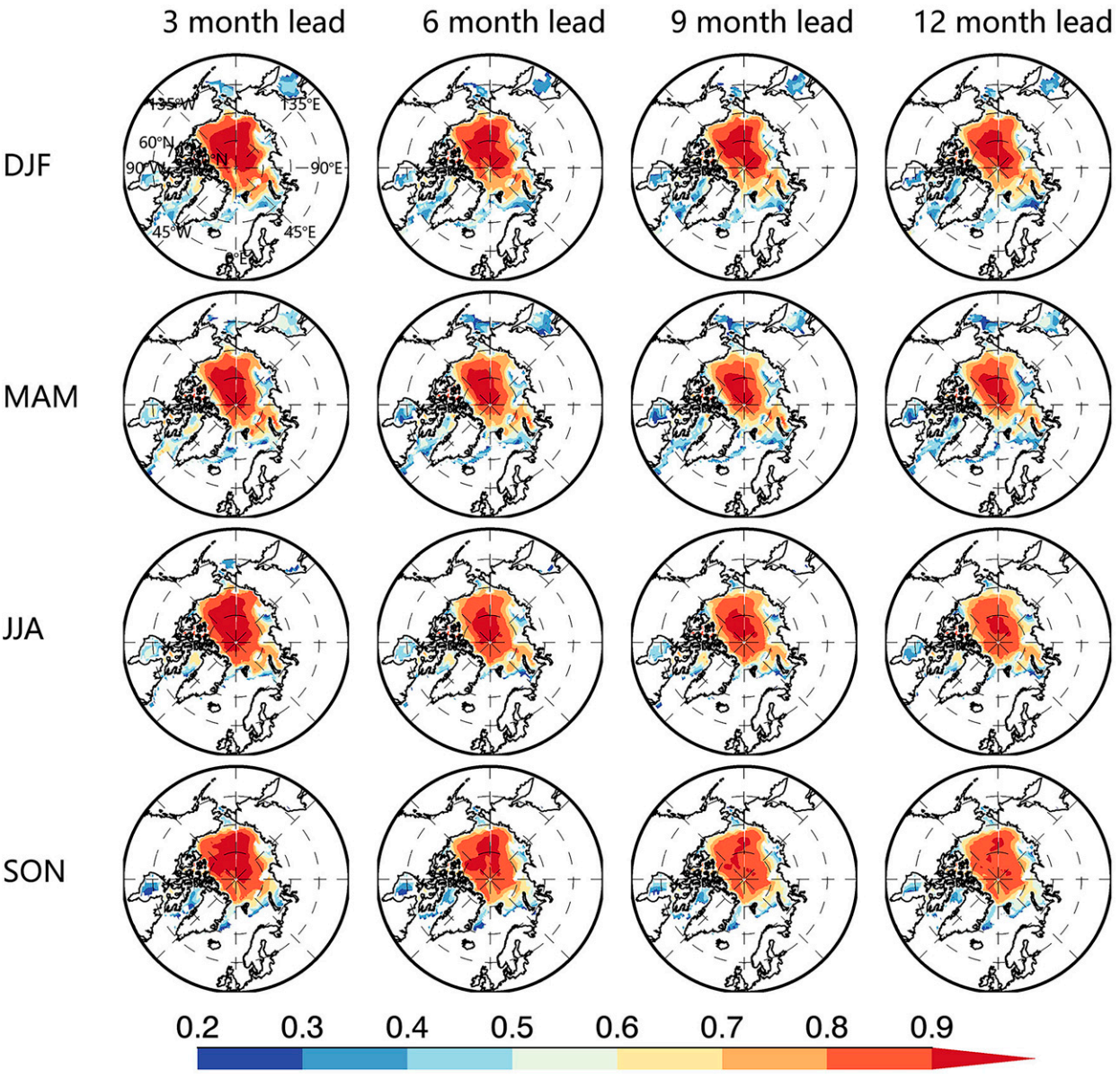

FIG. 4. Cross-validated model skill measured by ACC between SIT predictions and PIOMAS SIT anomalies as a function of target seasons and lead months. Only correlations significantly above 95% confidence level based on Student's *t* test are shaded.

seas for all seasons, which is consistent with the results of Tietsche et al. (2014). The magnitudes of RMSE remain at roughly the same level from 3- to 12-month leads in most locations. In addition, the error magnitudes in summer are the largest but still smaller than the SIT standard deviation (Fig. S1).

To show the regional and seasonal prediction skill for Arctic SIT total anomalies, we averaged the ACC in each region for all target months and lead months (Fig. 6). The result shows that each region displays a unique ACC feature. Skill is high (0.7–0.8) even up to 12-month leads in the central Arctic, East Siberian Sea, Chukchi Sea, and Beaufort Sea, which may be partially attributed to SIT trends and the ability of the Markov model to capture the trends and variability. The model in other marginal seas also performed well with an ACC of 0.5–0.6. Nevertheless, the skill is generally lower than 0.3 in peripheral seas including the Greenland Sea, Sea of Okhotsk, and Bering Sea, especially in summer. These regions are almost ice-free in summer, which cannot provide enough SIT information to the model. Also, the model performance is further evaluated against anomaly persistence (Fig. 6 and Fig. S6). The prediction skill of the Markov model exceeds that of an SIT persistence forecast in most regions of the Arctic, especially at 2–12-month leads. The model skill does not exceed persistence in the Canadian Archipelago and Baffin Bay during autumn when ice disappears. Furthermore, Arctic

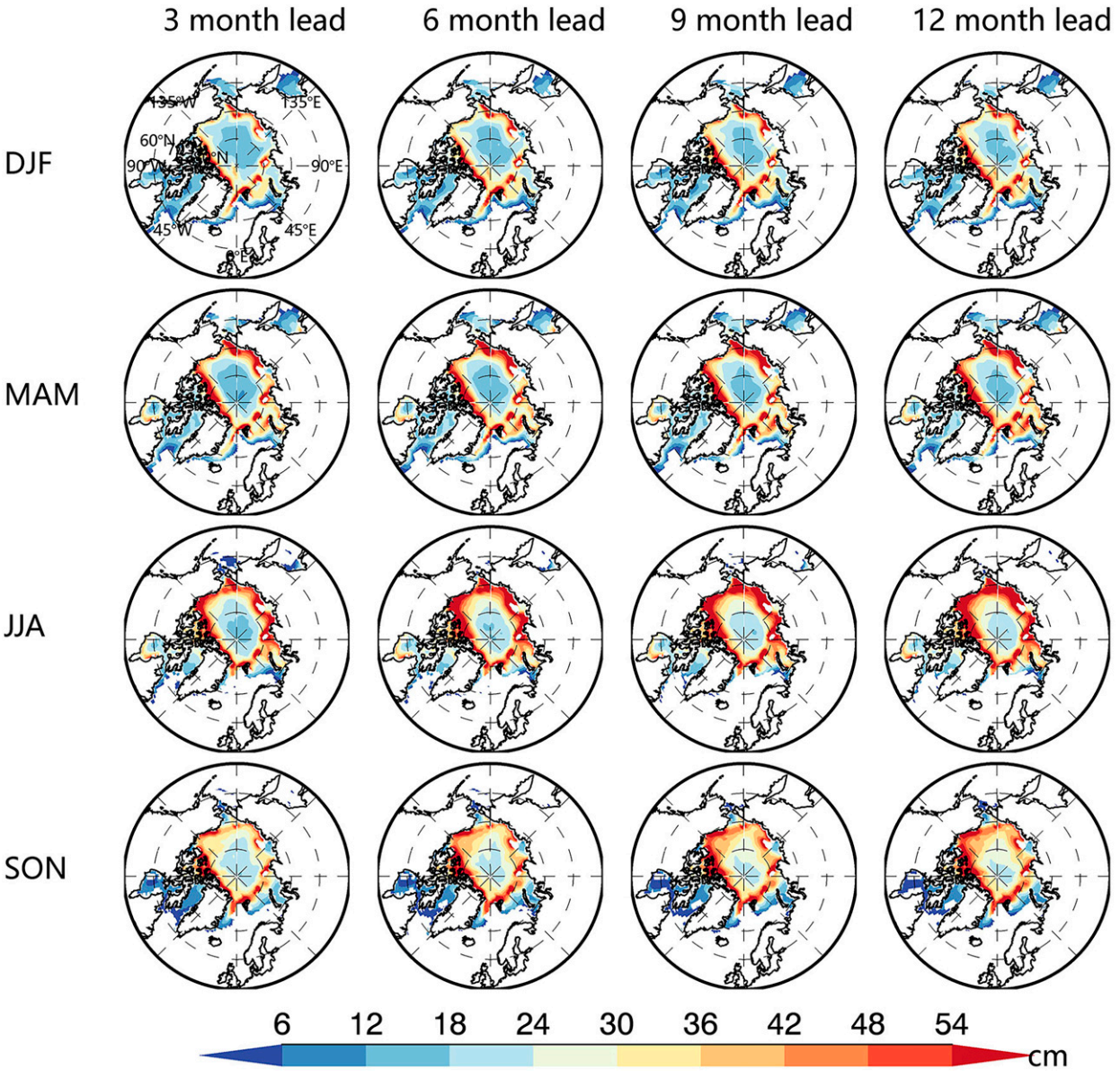

FIG. 5. As in Fig. 4, but for RMSEs.

sea ice has experienced a well-known declining trend over the last four decades. Specifically, September SIE (SIC) declined at $-0.81\ \text{km}^2\ \text{yr}^{-1}$ ($-12.7\%\ \text{decade}^{-1}$) during 1979–2021 (Meier et al. 2021). SIT has been decreasing at a rate from -3 to $-4\ \text{cm yr}^{-1}$ in most regions of the Arctic (Fig. S1a). Figure S2 shows that dimensionless SIT trends in the Arctic basin are a large part of SIT variabilities, which could largely contribute to the SIT prediction in the Markov model. Thus, it is worth evaluating the contribution of long-term SIT trends to the Markov model skill.

5. Contribution of SIT trends to prediction skill

To evaluate the contribution of monthly trends to the Markov model skill, we conducted a postprediction analysis in which respective monthly trends were removed from the initial SIT anomaly and predictions in each Arctic region. The detrended ACC thereby removes skill associated with secular trends and focuses on interannual anomalies. Although the model skill is significantly reduced for all seasons after a linear detrending, they are still high in the Arctic basin including the central Arctic, Beaufort Sea, East Siberian Sea, and Chukchi Sea (Fig. 7). The prediction skill is higest in the Beaufort Sea. The ACCs are above 0.6 up to 12-month leads in winter and up to 4-month leads in summer, representing skillful predictions. The ACC in the central Arctic is generally 0.1 lower than that in the Beaufort Sea. The East Siberian Sea and Chukchi Sea have a similar ACC pattern in which prediction skill is significant for up to 12-month leads in the cold seasons

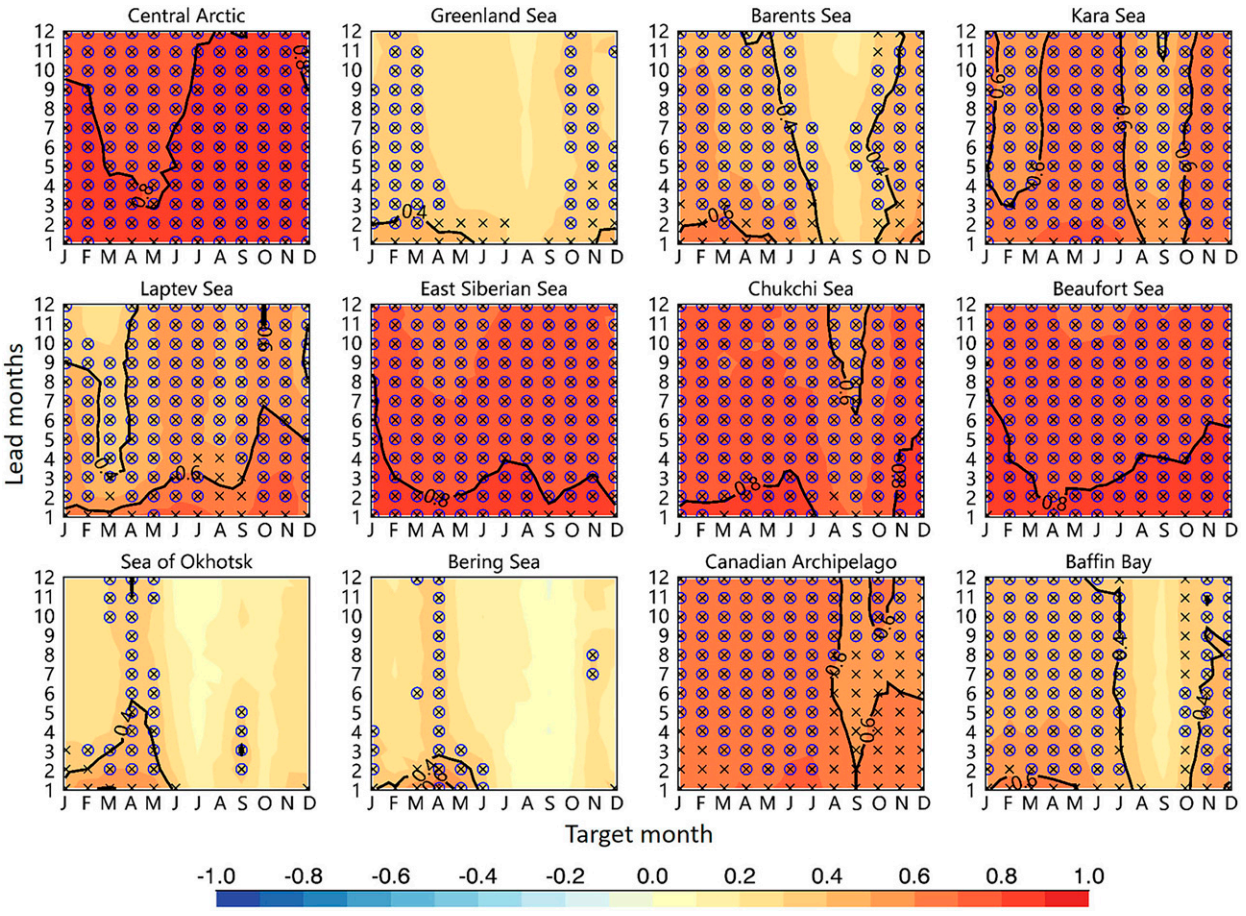

FIG. 6. Seasonal SIT prediction skill (ACC) in Arctic regions. Black crosses represent ACCs significantly above 95% confidence level, and blue circles marked on crosses indicate the months in which the model's skill exceeds the persistence forecast. The contours of 0.4, 0.6, and 0.8, are superimposed on images.

and up to 6-month leads in the warm seasons. Canadian Archipelago and Baffin Bay also have a similar correlation structure that reasonable prediction skill only occurs in the cold seasons. In the Kara Sea, the model has moderate skill in fall and spring. The ACC in the peripheral seas is lower than 0.4 in general, especially in the warm season when ice melts away. The model skill in the cold season is generally higher than in the warm season after trend removal. Overall, the Markov model has the ability to capture predictable SIT internal variability in the Arctic.

The contributions of monthly SIT trends to the model skill are described by the difference between ACCs in Figs. 6 and 7. The results show that the SIT trends contribute largely to the model skill for all seasons in the central Arctic and most marginal seas, especially at longer lead months (6–12). Averaging the ACC reductions (Fig. 8) at all lead times and target months, it was reduced by 40%, 55%, 49%, and 47% in the central Arctic, Laptev Sea, East Siberian Sea, and Chukchi Sea, respectively, after the trend was removed (Table 2). The mean ACC was reduced by 33%, 40%, 38%, and 38% in those regions over 1–6-month leads. Monthly trends also contribute 80% of skill in Canadian Archipelago prediction in the warm seasons and contribute 48% of skill in Kara Sea summer predictions.

Interestingly, the SIT trends make insignificant contributions to the prediction skill in the Beaufort Sea, which contrasts with other marginal seas. The average trend of SIT anomalies in the Beaufort Sea is equivalent to that of the Chukchi Sea and smaller than that of the East Siberian Sea, while the average standard deviation of the SIT anomalies is the largest among all Arctic regions. In other words, the SIT in the Beaufort Sea has the largest interannual variability, which could contribute significantly to the SIT predictability. Interannual variability of SIT in the Beaufort Sea is associated with Beaufort Gyre (BG) (Petty 2018; Mahoney et al. 2019). The BG is an anticyclonic ice–ocean circulation system and is driven by the semipermanent Beaufort High. The BG is a prominent sea ice and ocean surface circulation feature of the Arctic Ocean and is thought to play a significant role in regulating Arctic sea ice variability (Armitage et al. 2020). Generally, the anticyclonic winds associated with Beaufort high set sea ice in motion. During the anticyclonic circulation regime, sea ice has the opportunity to thicken through ice growth and deformation due to Ekman convergence (Petty

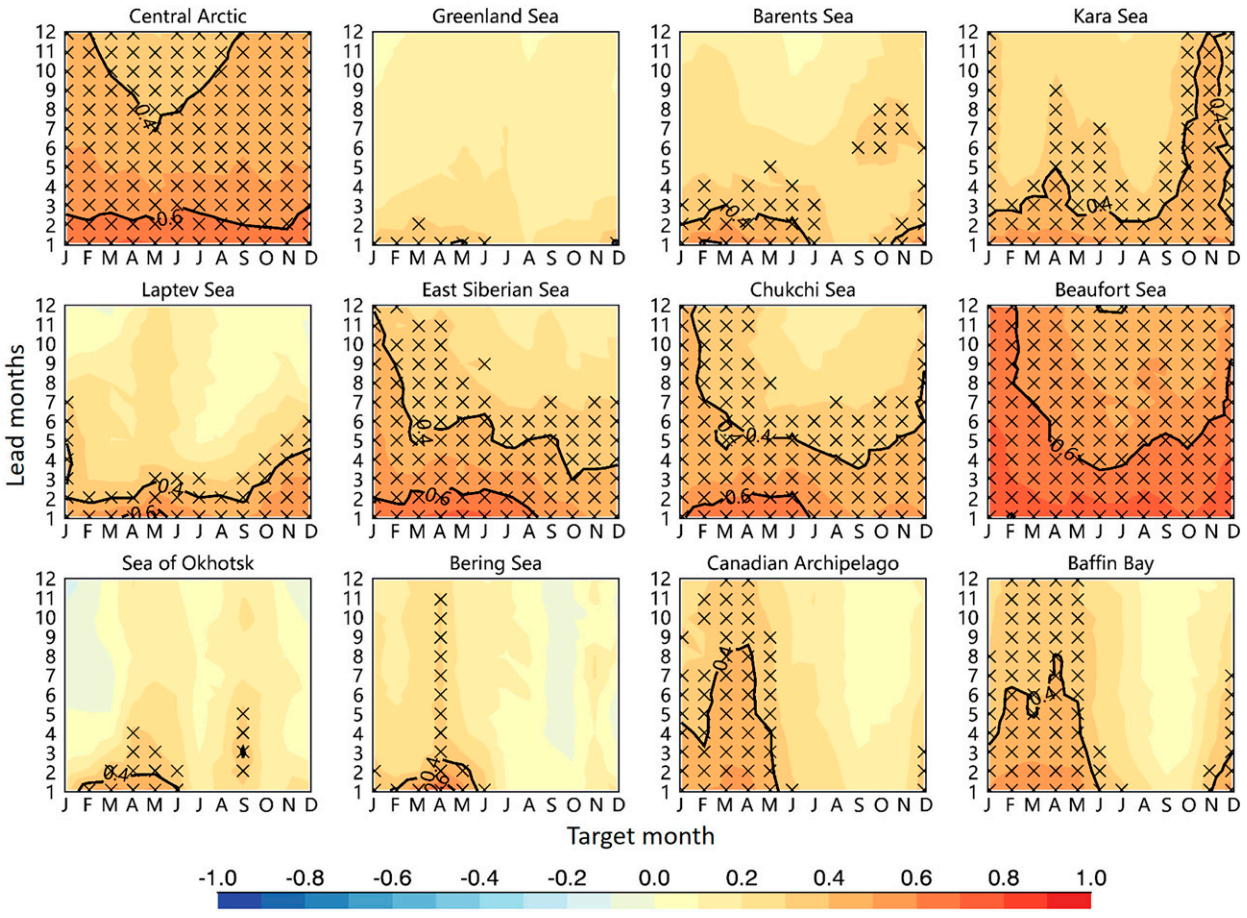

FIG. 7. Seasonal SIT prediction skill measured by ACC between detrended initial SIT and detrended predictions. Black crosses represent ACCs significantly above 95% confidence level. The contours of 0.4 and 0.6, are superimposed on images.

et al. 2016). While weakening or even reverse of the anticyclonic circulation regime can enhance sea ice export from the Beaufort Sea and thin the SIT. Therefore, the variability of SIT driven by BG is relatively large in the Beaufort Sea, which predominantly contributes to the prediction skill.

6. Discussion

Due to the lack of long records of SIT observations (Lindsay and Schweiger 2015; Dawson et al. 2022; Fiedler et al. 2022), here we used the model product from PIOMAS as the observed Arctic SIT. To evaluate the reliability of the data, we further used altimeter-based satellite observations from CS2SMOS in wintertime for the period 2010–20 to verify the PIOMAS SIT, although earlier works have proven that PIOMAS is reliable (Laxon et al. 2013; Mu et al. 2018; Ponsoni et al. 2019; Chylek et al. 2022). The results show that the spatial features of the SIT standard deviation from the two datasets are similar (Figs. 9a,c). Large SIT variability with a monthly standard deviation greater than 0.6 m, mainly occurs in north coast of Canadian Arctic Archipelago (CAA) and Greenland, while weak variability mainly occurs in the peripheral seas. The main differences between the two are that SIT variability from PIOMAS is relatively small in the Greenland Sea and large in north side of islands in the Arctic Ocean such as New Siberian Island, North Island, and Franz Josef Land.

The SIT climatologies from the two datasets are also similar in magnitude in February when sea ice is thickest (Figs. 9b,d). Thicker ice (>2.5 m) mainly distributes along the band north of CAA and Greenland, where multiyear ice dominates the thickness of sea ice. Thin ice (<1 m) is mainly composed of seasonal ice spreads in peripheral seas including the Barents Sea, Bering Sea, and Sea of Okhotsk. Compared with CS2SMOS, PIOMAS sea ice is relatively thinner in the central Arctic and Greenland Sea and thicker in other regions. In addition, the correlations between the two datasets are generally high, especially in the marginal seas and peripheral seas (Fig. 9e). RMSEs are consistent with ACC: high correlations correspond to low RMSEs, and vice versa, although minor inconsistencies occur in some regions (Fig. 9f). Thus these analyses suggest that the PIOMAS SIT captures the main characteristics of the satellite observed SIT.

To check the robustness of our model, we further use sevenfold cross validation to evaluate the prediction skill of the optimal model that V3M13, V3M14, V3M9, and V9M9 as the best models for winter, spring, summer, and autumn, respectively.

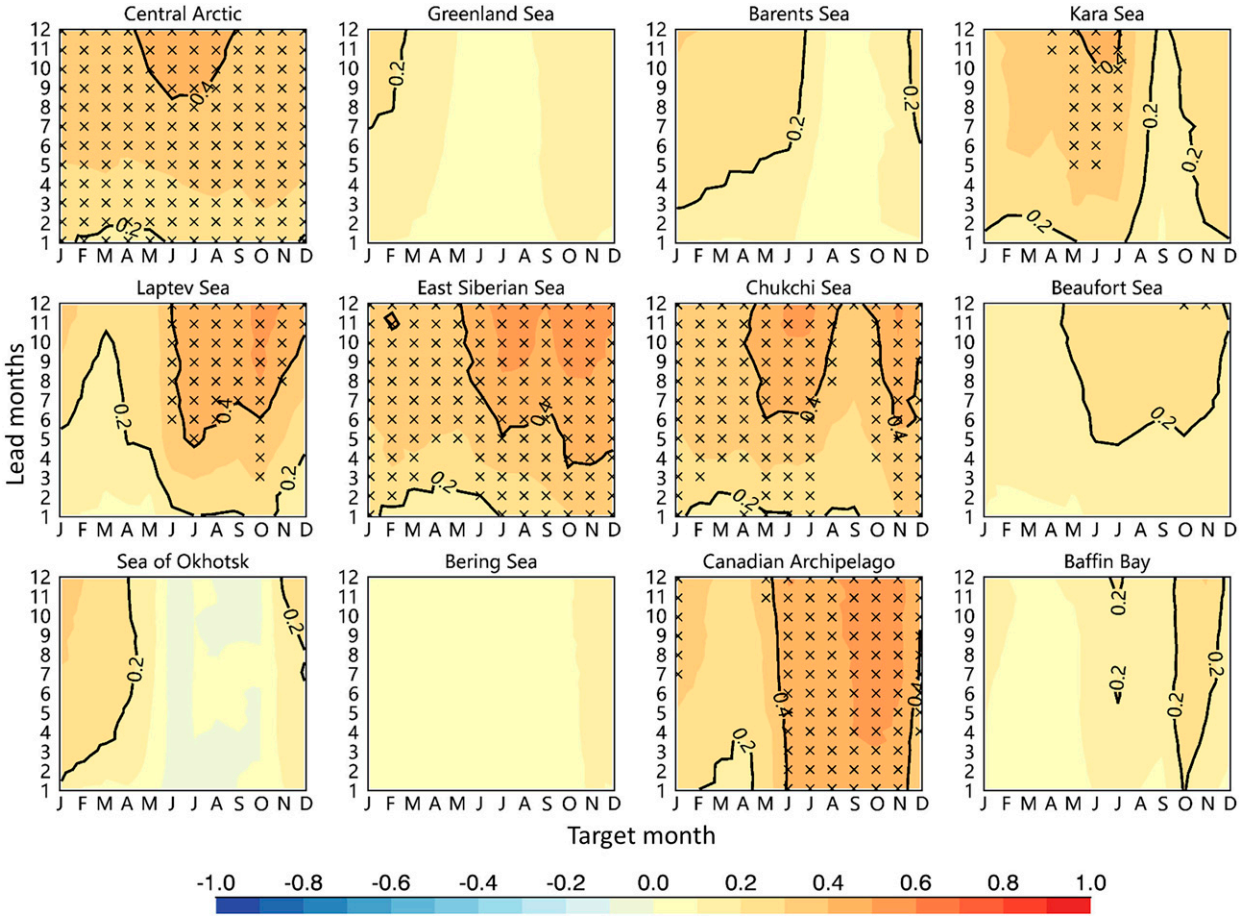

FIG. 8. Skill differences between Figs. 6 and 7. Black crosses indicate that ACC differences are significant above 95% confidence level. The contours of 0.2 and 0.4, are superimposed.

In sevenfold cross validation, the 42-yr time series is partitioned into seven equal-sized subsamples. Of the seven subsamples, a single subsample (6-yr time series) is retained as the validation data for testing the model, and the remaining six subsamples are used as a training set. The cross-validation process is then repeated seven times, with each of the seven subsamples used exactly once as the validation set. Sevenfold cross validation is equivalent to leave-6-years-out cross validation.

TABLE 2. Mean ACCs between prediction and PIOMAS SIT when monthly SIT trends are retained or removed in each Arctic region. Here mean ACCs are calculated from 1- to 12-month leads and from 1- to 6-month leads, respectively. "Reduction" denotes contribution of monthly SIT trends to ACCs.

	1–12 lead months			1–6 lead months		
Arctic regions	ACC	Detrended ACC	Reduction	ACC	Detrended ACC	Reduction
Central Arctic	0.81	0.49	40%	0.84	0.56	33%
Greenland Sea	0.3	0.18	41%	0.32	0.22	33%
Barents Sea	0.43	0.27	38%	0.46	0.33	28%
Kara Sea	0.61	0.35	43%	0.63	0.4	37%
Laptev Sea	0.52	0.23	55%	0.57	0.35	40%
East Siberian Sea	0.75	0.39	49%	0.79	0.49	38%
Chukchi Sea	0.73	0.38	47%	0.76	0.47	38%
Beaufort Sea	0.77	0.59	23%	0.8	0.66	18%
Sea of Okhotsk	0.25	0.14	45%	0.29	0.2	32%
Bering Sea	0.2	0.15	26%	0.22	0.18	21%
Canadian Archipelago	0.64	0.25	61%	0.65	0.29	55%
Baffin Bay	0.41	0.28	33%	0.44	0.32	27%

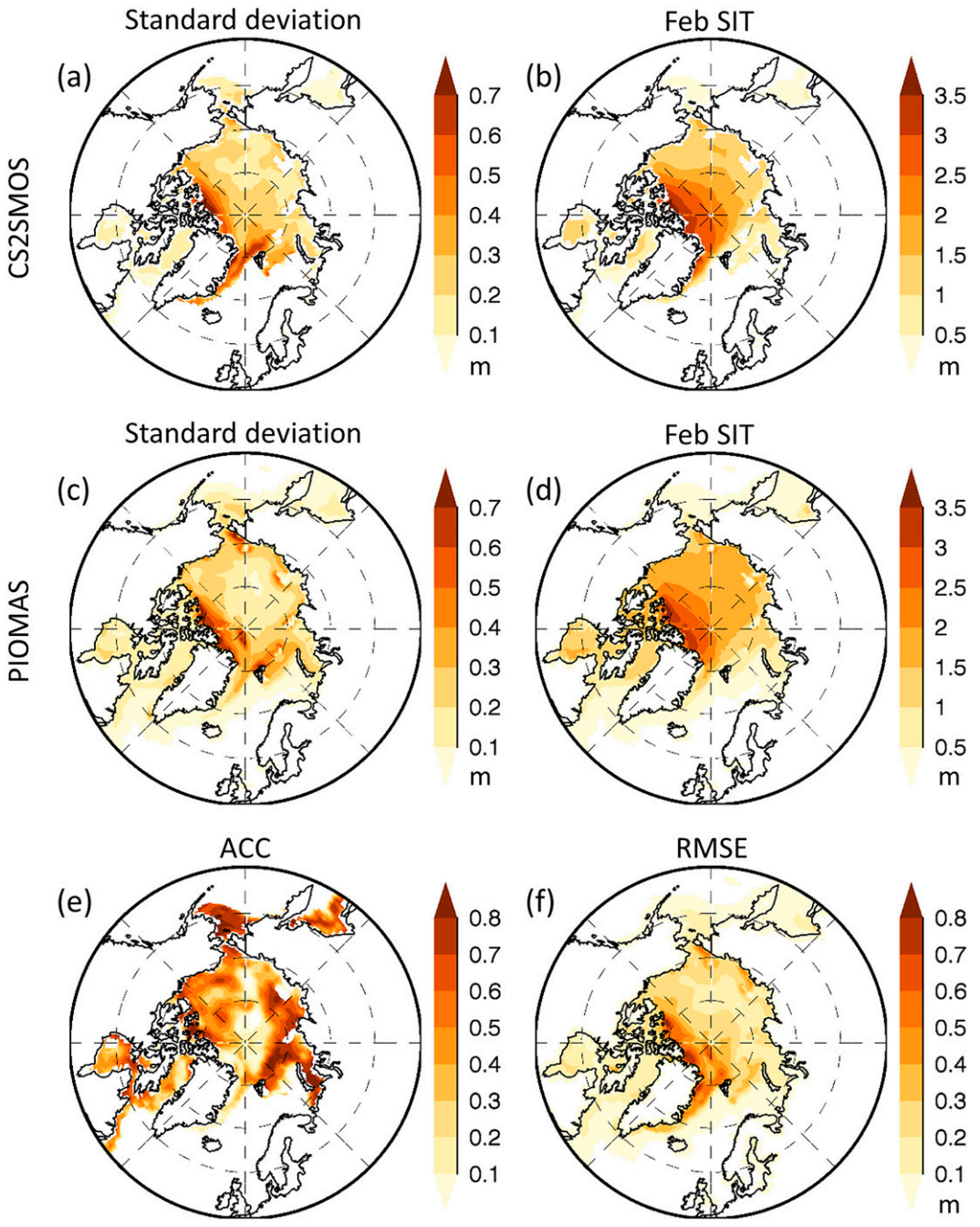

FIG. 9. Comparison of winter SITs between CS2SMOS satellite observations and PIOMAS model product from 2010 to 2020. (a) Standard deviation of CS2SMOS SIT monthly mean anomalies in the cold season (November–March). (b) CS2SMOS SIT in February averaged over the period. (c),(d) As in (a) and (b), but for PIOMAS SIT. (e) Anomaly correlation coefficient (ACC) between two SIT monthly mean anomalies. (f) As in (e), but for RMSE.

The result shows that the prediction skill from leave-6-years-out cross validation shows a similar pattern as the skill from leave-1-year-out cross validation but with a roughly 0.1 lower ACC (Figs. 10 and 4). High forecast skill are also concentrated in the central Arctic basin. The model skill decreases continuously with an increase in lead months, but it is still significant even at 12-month leads for all seasons in the Arctic basin. In addition, RMSEs from the two cross validations also have similar patterns, although the former has 6 cm larger (Fig. S5 and Fig. 5). These above results support the robustness of the model.

To check if the Markov model skill is sensitive to SIT anomaly time series weights, we calculated the seasonal SIT

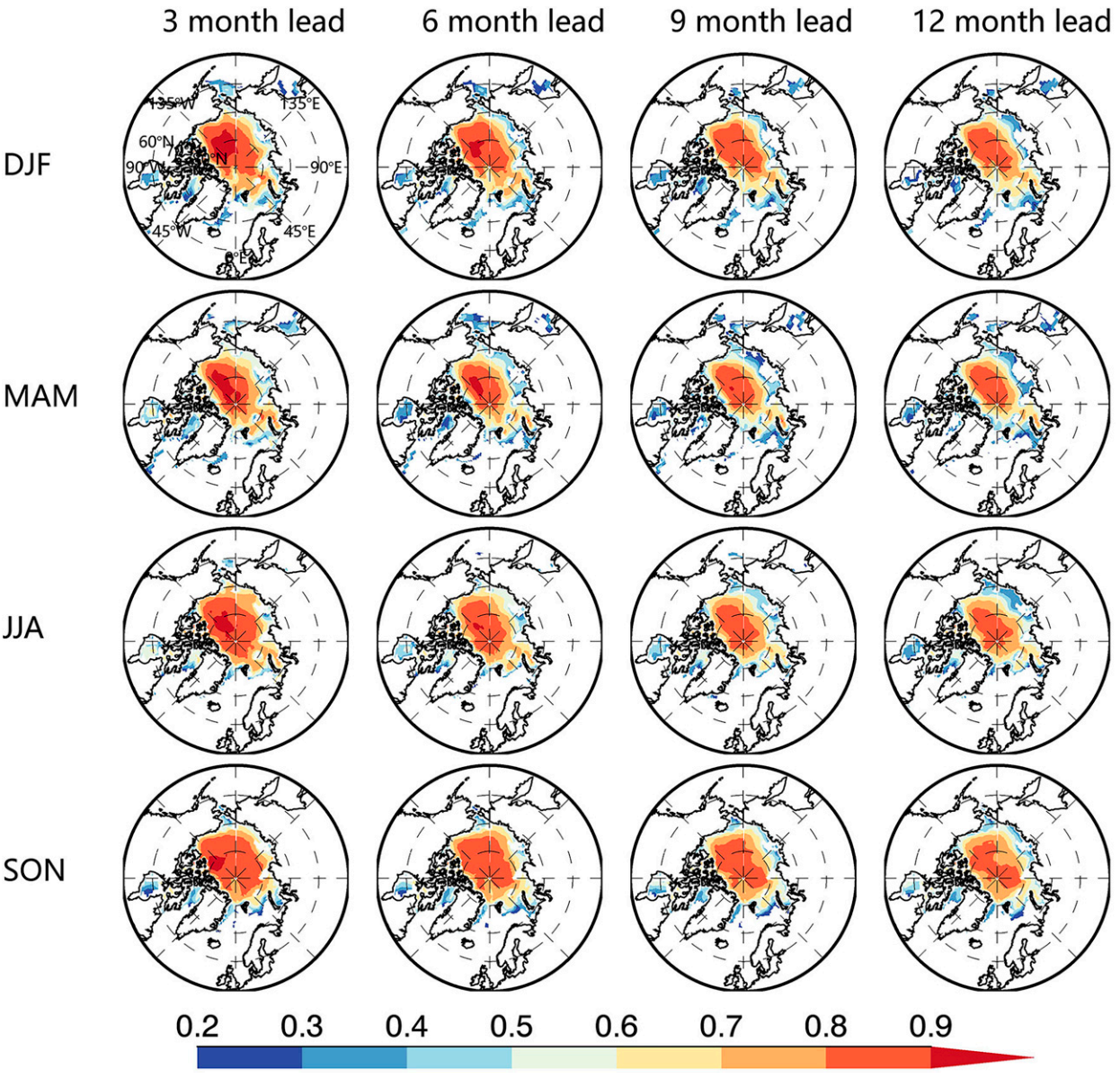

FIG. 10. As in Fig. 4, but for the case where the prediction skill (ACC) is calculated from sevenfold cross validation.

prediction skill (ACC) of the model, in which SIT anomaly time series is unweighted in calculating MEOFs. The results show that the ACC patterns and magnitudes of Fig. S7 (unweighted) are very similar to those of Fig. 6 (weighted) for all Arctic regions, which reflects that the influence of weighting the SIT anomaly time series by a factor of 2 on the model skill is not fundamental. Since we emphasize SIT, we keep the weight in calculating MEOFs.

We constructed a Markov model with an optimal variable combination. However, this model is not perfect because it is challenging for us to test all variable combinations in nature. In other words, it does not rule out the existence of other variable combinations, which can improve the SIT prediction skill of the Markov model. In addition, we find that the contributions of OHC to the SIT prediction skill are more significant than those of all atmospheric variables on a seasonal scale (Fig. S4). It may be that the atmospheric variabilities are mainly on shorter time scales relative to changes in sea ice and ocean, and the ocean dominates the seasonal variability of SIT with massive heat and significant seasonal signals. Guemas et al. (2016a) also suggested that although the atmospheric process stands as a major driver of Arctic sea ice, its low predictability beyond 1 or 2 weeks makes the atmosphere unable to be a crucial source of sea ice predictability. Although surface radiation flux can provide some skill for the model, the contribution is much smaller than that of OHC. Adding GPH and winds to the Markov model could even reduce the SIT prediction skill, implying that the Markov model cannot well capture the SIT prediction skill

from dynamic signals in pan-Arctic averages, even though these dynamic factors play a vital role in Arctic SIT regional or local changes. Blanchard-Wrigglesworth et al. (2011) also pointed out that atmospheric circulation has little contribution to sea ice persistence in the seasonal time scale.

Many studies have shown evidence for an Arctic sea ice spring predictability barrier that forecasts of September sea ice initialized prior to May are substantially less skillful than forecasts initialized after May (Day et al. 2014; Bushuk et al. 2017; Bonan et al. 2019; Bushuk et al. 2020). This spring predictability barrier especially exists across the Laptev, East Siberian, and Beaufort Seas (Bushuk et al. 2019). However, Arctic SIT forecasts by the Markov model are capable of breaking through this spring predictability barrier, which is likely attributed to SIT and OHC long persistence and the capability of the Markov model to capture the covaraibility between SIT and OHC. Unlike the SIC prediction that the model skill in the warm season is substantially higher than that of in the cold season (Wang et al. 2022a), the SIT prediction skill is high in the cold season. This may be mainly attributed to the large SIT variability in the cold season. In addition, SIT persists much longer than SIC (Blanchard-Wrigglesworth et al. 2011). The persistence time scale of SIT is approximately 1 year in the central Arctic and a few months in the seasonal ice zone, while the persistence of nondetrended SIC anomalies is a 1–5-month time scale. With global warming and polar amplification, Arctic surface air temperature will continuously increase, and along with it, the OHC of the Arctic Ocean in the coming decades. Such an Arctic climate system will lead to thinner sea ice and shrinking SIT persistence. Thus, SIT predictability might be further reduced in the future.

7. Conclusions

In this study, we developed a linear Markov model configured for Arctic SIT seasonal prediction and tested the performance of physically relevant predictors. The model was constructed in the MEOF space and captured the covariability of the ocean–ice–atmosphere coupled Arctic climate system with nine variables: SIT, SIC, OHC, SST, SAT, SNRF, SNTF, GPH, and winds. Based on cross-validation experiments, we chose V3M13, V3M14, V3M9, and V9M9 as the best models for winter, spring, summer, and autumn, respectively. V3 is composed of SIT and OHC, and V9 is composed of SIT, OHC, SST, and SAT. The two variable combinations are both weighted toward thermodynamic processes. The cross-validation experiments also showed that the model skill comes primarily from SIT itself. OHC generally contributes more SIT prediction skill than other variables.

The SIT prediction skill was evaluated in each Arctic region and for all seasons. Similar to the SIC prediction, the SIT prediction by the Markov model is not sensitive to the number of MEOF modes retained, which indicates that the performance of this Markov model is robust and can be determined by a small subset of leading modes. More modes were also needed in the cold season to capture the predictable SIT signal. In addition, with an increase in the number of lead months, model skill decreases continuously. SIT prediction has better skill in the cold season than in the warm season, which is opposite to SIC prediction. Spatially, each Arctic region displays a unique ACC feature when linear trends are retained in SIT anomalies and predictions. Skill measured by ACCs is high (0.7–0.8) in the central Arctic, East Siberian Sea, Chukchi Sea, and Beaufort Sea. The model in other marginal seas also performed well with an ACC of 0.5–0.6. Nevertheless, the skill is generally lower than 0.3 in peripheral seas, including the Greenland Sea, Sea of Okhotsk, and the Bering Sea, especially in summer because those regions are almost ice-free in summer, which cannot provide enough SIT variability for the model to capture and predict.

The monthly SIT trends contribute largely to the model skill for all seasons in the central Arctic and most marginal seas. Trend removal from predictions and observations results in a 40%, 55%, 49%, and 47% reduction of the mean ACC for the central Arctic, Laptev Sea, East Siberian Sea, and Chukchi Sea at 1–12-month lead. Trend's contribution to the model skill increases continuously with the number of lead months. The mean ACC actually reduced by 33%, 40%, 38%, and 38% in those regions over 1–6-month leads. Interestingly, the SIT trends make a minor contribution to prediction skill in the Beaufort Sea, which is drastically different from other marginal seas. Although the model skill is significantly reduced for all seasons after linear trend removal, the model is still skillful in many Arctic regions. The ACCs are approximately 0.6 up to 4-month leads, and 0.4 up to 12-month leads in the Beaufort Sea where the skill is the highest among all the Arctic regions. The ACC in the central Arctic is generally 0.1 lower than that in the Beaufort Sea. Moreover, the model's skill is higher than the SIT persistence skill in all Arctic regions at 2–12-month leads, revealing the Markov model's capability of capturing predictable SIT internal variability beyond linear trends.

The advantages of the SIT Markov model can be summarized as follows. First, the Markov model for SIT prediction is built on multivariate spaces, which can capture the covariability in the ocean–ice–atmosphere coupled system instead of linearly regressing on individual predictors. In particular, the covariability of SIT and OHC contributes to long-lead SIT predictability. Second, we use only the first 9–14 leading MEOF modes to filter out unpredictable small-scale features and pay more attention to the predictable signals. Finally, the model consists of four seasonal modules with different sets of predictors, accommodating seasonally varying driving processes and avoiding weak signal seasons dominated by strong signal seasons. Benefiting from the above advantages, the Markov model can capture the melt-to-growth season reemergence of SIT predictability, shows no spring predictability barrier, and is an effective tool for seasonal predictions. Further investigation is also required in order to establish a systematic physical mechanism for explaining the nonexistence of a spring predictability barrier in our Markov model predictions.

Combined with the previous work (Wang et al. 2022a), the successful applications of the Markov model in SIT and SIC predictions also reflect that spatiotemporal characteristics of SIC and SIT predictability are distinct. These results give us

many new insights. This study expands the prediction of SIC and SIE to a new dimension. SIT prediction is more valuable for navigating in polar seas, which provides information for fuel assumption estimates of ice breakers. The knowledge of SIT and SIC also allows us to estimate volume of sea ice. In addition, year-round satellite SIT records from *CryoSat-2* have recently been generated (Landy et al. 2022), giving us with more advanced satellite SIT data to predict sea ice or evaluate sea ice predictions in the future, although its time series currently is too short for an application at the seasonal scale. The findings and products from this study will further support us in investigation of Arctic SIV predictions in future work.

Acknowledgments. This work is supported by the Natural Science Foundation of Shandong Province, China (ZR2021QD059; ZR2020MD100); National Natural Science Foundation of China (42106223); China Postdoctoral Science Foundation (2020TQ0322); Laoshan Laboratory (LSKJ202203003; LSKJ202202303); Open Funds for the Key Laboratory of Marine Geology and Environment, Institute of Oceanology, and Chinese Academy of Sciences (MGE2021KG15; MGE2020KG04). Yuan is supported by the Lamont-Doherty Earth Observatory of Columbia University with a private donation (Ying).

Data availability statement. Monthly SITs from the Pan-Arctic Ice-Ocean and Assimilating System (PIOMAS) can be obtained from the Polar Science Center (PSC) (http://psc.apl.uw.edu/research/projects/arctic-sea-ice-volume-anomaly/data/model_grid). The CS2SMOS SITs available at https://data.seaiceportal.de/data/cs2smos_awi/v204/n/. Monthly SICs from the National Snow and Ice Data Center (NSIDC) are available at https://n5eil01u.ecs.nsidc.org/PM/NSIDC-0079.003/. The ocean heat content in the upper 300 m, sea surface temperature, surface air temperature, surface net radiative flux, surface net turbulent heat flux, 850-hPa geopotential height, and 850-hPa wind vector from ERA5 can be obtained from the ECMWF (https://cds.climate.copernicus.eu/cdsapp#!/search?type=dataset).

REFERENCES

Andersson, T. R., and Coauthors, 2021: Seasonal Arctic sea ice forecasting with probabilistic deep learning. *Nat. Commun.*, **12**, 5124, https://doi.org/10.1038/s41467-021-25257-4.

Armitage, T. W. K., G. E. Manucharyan, A. A. Petty, R. Kwok, and A. F. Thompson, 2020: Enhanced eddy activity in the Beaufort Gyre in response to sea ice loss. *Nat. Commun.*, **11**, 761, https://doi.org/10.1038/s41467-020-14449-z.

Ballinger, T. J., and Coauthors, 2021: Surface air temperature. NOAA Tech. Rep. OAR ARC 21-02, 7 pp., https://repository.library.noaa.gov/view/noaa/34475.

Barnston, A. G., and C. F. Ropelewski, 1992: Prediction of ENSO episodes using canonical correlation analysis. *J. Climate*, **5**, 1316–1345, https://doi.org/10.1175/1520-0442(1992)005<1316:POEEUC>2.0.CO;2.

Bhatt, U. S., and Coauthors, 2022: 2021 sea ice outlook post-season report. ARCUS, https://www.arcus.org/sipn/sea-ice-outlook/2021/post-season.

Blackport, R., J. A. Screen, K. van der Wiel, and R. Bintanja, 2019: Minimal influence of reduced Arctic sea ice on coincident cold winters in mid-latitudes. *Nat. Climate Change*, **9**, 697–704, https://doi.org/10.1038/s41558-019-0551-4.

Blanchard-Wrigglesworth, E., K. C. Armour, C. M. Bitz, and E. Deweaver, 2011: Persistence and inherent predictability of Arctic sea ice in a GCM ensemble and observations. *J. Climate*, **24**, 231–250, https://doi.org/10.1175/2010JCLI3775.1.

——, R. I. Cullather, W. Wang, J. Zhang, and C. M. Bitz, 2015: Model forecast skill and sensitivity to initial conditions in the seasonal sea ice outlook. *Geophys. Res. Lett.*, **42**, 8042–8048, https://doi.org/10.1002/2015GL065860.

Bonan, D. B., M. Bushuk, and M. Winton, 2019: A spring barrier for regional predictions of summer Arctic sea ice. *Geophys. Res. Lett.*, **46**, 5937–5947, https://doi.org/10.1029/2019GL082947.

Bushuk, M., and D. Giannakis, 2017: The seasonality and interannual variability of Arctic sea ice reemergence. *J. Climate*, **30**, 4657–4676, https://doi.org/10.1175/JCLI-D-16-0549.1.

——, R. Msadek, M. Winton, G. A. Vecchi, R. Gudgel, A. Rosati, and X. Yang, 2017: Skillful regional prediction of Arctic sea ice on seasonal timescales. *Geophys. Res. Lett.*, **44**, 4953–4964, https://doi.org/10.1002/2017GL073155.

——, ——, ——, G. Vecchi, X. Yang, A. Rosati, and R. Gudgel, 2019: Regional Arctic sea-ice prediction: Potential versus operational seasonal forecast skill. *Climate Dyn.*, **52**, 2721–2743, https://doi.org/10.1007/s00382-018-4288-y.

——, M. Winton, D. B. Bonan, E. Blanchard-Wrigglesworth, and T. L. Delworth, 2020: A mechanism for the Arctic sea ice spring predictability barrier. *Geophys. Res. Lett.*, **47**, e2020GL088335, https://doi.org/10.1029/2020GL088335.

——, and Coauthors, 2021: Seasonal prediction and predictability of regional Antarctic sea ice. *J. Climate*, **34**, 6207–6233, https://doi.org/10.1175/JCLI-D-20-0965.1.

Cai, Q., J. Wang, D. Beletsky, J. Overland, M. Ikeda, and L. Wan, 2021: Accelerated decline of summer Arctic sea ice during 1850–2017 and the amplified Arctic warming during the recent decades. *Environ. Res. Lett.*, **16**, 034015, https://doi.org/10.1088/1748-9326/abdb5f.

Chen, J., and Coauthors, 2021: Perspectives on future sea ice and navigability in the Arctic. *Cryosphere*, **15**, 5473–5482, https://doi.org/10.5194/tc-15-5473-2021.

Cheng, L., G. Wang, J. P. Abraham, and G. Huang, 2018: Decadal ocean heat redistribution since the late 1990s and its association with key climate modes. *Climate*, **6**, 91, https://doi.org/10.3390/cli6040091.

Chi, J., and H.-c. Kim, 2017: Prediction of arctic sea ice concentration using a fully data driven deep neural network. *Remote Sens.*, **9**, 1305, https://doi.org/10.3390/rs9121305.

Chylek, P., C. Folland, J. D. Klett, M. Wang, N. Hengartner, G. Lesins, and M. K. Dubey, 2022: Annual mean Arctic amplification 1970–2020: Observed and simulated by CMIP6 climate models. *Geophys. Res. Lett.*, **49**, e2022GL099371, https://doi.org/10.1029/2022GL099371.

Cohen, J., and Coauthors, 2020: Divergent consensuses on Arctic amplification influence on midlatitude severe winter weather. *Nat. Climate Change*, **10**, 20–29, https://doi.org/10.1038/s41558-019-0662-y.

Comiso, J. C., 2017: Bootstrap sea ice concentrations from Nimbus-7 SMMR and DMSP SSM/I-SSMIS, version 3. NASA National

Snow and Ice Data Center, accessed 21 April 2023, https://doi.org/10.5067/7Q8HCCWS4I0R.

Dai, P., Y. Gao, F. Counillon, Y. Wang, M. Kimmritz, and H. R. Langehaug, 2020: Seasonal to decadal predictions of regional Arctic sea ice by assimilating sea surface temperature in the Norwegian climate prediction model. *Climate Dyn.*, **54**, 3863–3878, https://doi.org/10.1007/s00382-020-05196-4.

Dawson, G., J. Landy, M. Tsamados, A. S. Komarov, S. Howell, H. Heorton, and T. Krumpen, 2022: A 10-year record of Arctic summer sea ice freeboard from CryoSat-2. *Remote Sens. Environ.*, **268**, 112744, https://doi.org/10.1016/j.rse.2021.112744.

Day, J. J., S. Tietsche, and E. Hawkins, 2014: Pan-Arctic and regional sea ice predictability: Initialization month dependence. *J. Climate*, **27**, 4371–4390, https://doi.org/10.1175/JCLI-D-13-00614.1.

England, M. R., I. Eisenman, N. J. Lutsko, and T. J. W. Wagner, 2021: The recent emergence of Arctic amplification. *Geophys. Res. Lett.*, **48**, e2021GL094086, https://doi.org/10.1029/2021GL094086.

Fauchald, P., P. Arneberg, J. B. Debernard, S. Lind, E. Olsen, and V. H. Hausner, 2021: Poleward shifts in marine fisheries under Arctic warming. *Environ. Res. Lett.*, **16**, 074057, https://doi.org/10.1088/1748-9326/ac1010.

Fiedler, E. K., M. J. Martin, E. Blockley, D. Mignac, N. Fournier, A. Ridout, A. Shepherd, and R. Tillingand, 2022: Assimilation of sea ice thickness derived from CryoSat-2 along-track freeboard measurements into the Met Office's Forecast Ocean Assimilation Model (FOAM). *Cryosphere*, **16**, 61–85, https://doi.org/10.5194/tc-16-61-2022.

Francis, J. A., and S. J. Vavrus, 2012: Evidence linking Arctic amplification to extreme weather in mid-latitudes. *Geophys. Res. Lett.*, **39**, L06801, https://doi.org/10.1029/2012GL051000.

Gao, P. A., H. M. Director, C. M. Bitz, and A. E. Raftery, 2022: Probabilistic forecasts of Arctic sea ice thickness. *J. Agric. Biol. Environ. Stat.*, **27**, 280–302, https://doi.org/10.1007/s13253-021-00480-0.

Gregory, W., M. Tsamados, J. Stroeve, and P. Sollich, 2020: Regional September sea ice forecasting with complex networks and Gaussian processes. *Wea. Forecasting*, **35**, 793–806, https://doi.org/10.1175/WAF-D-19-0107.1.

Guarino, M.-V., and Coauthors, 2020: Sea-ice-free Arctic during the last interglacial supports fast future loss. *Nat. Climate Change*, **10**, 928–932, https://doi.org/10.1038/s41558-020-0865-2.

Guemas, V., and Coauthors, 2016a: A review on Arctic sea-ice predictability and prediction on seasonal to decadal timescales. *Quart. J. Roy. Meteor. Soc.*, **142**, 546–561, https://doi.org/10.1002/qj.2401.

——, M. Chevallier, M. Deque, O. Bellprat, and F. Doblas-Reyes, 2016b: Impact of sea ice initialization on sea ice and atmosphere prediction skill on seasonal timescales. *Geophys. Res. Lett.*, **43**, 3889–3896, https://doi.org/10.1002/2015GL066626.

Hersbach, H., and Coauthors, 2020: The ERA5 global reanalysis. *Quart. J. Roy. Meteor. Soc.*, **146**, 1999–2049, https://doi.org/10.1002/qj.3803.

Horvath, S., J. Stroeve, B. Rajagopalan, and W. Kleiber, 2020: A Bayesian logistic regression for probabilistic forecasts of the minimum September Arctic sea ice cover. *Earth Space Sci.*, **7**, e2020EA001176, https://doi.org/10.1029/2020EA001176.

Huntington, H. P., and Coauthors, 2015: Vessels, risks, and rules: Planning for safe shipping in Bering Strait. *Mar. Policy*, **51**, 119–127, https://doi.org/10.1016/j.marpol.2014.07.027.

Ionita, M., K. Grosfeld, P. Scholz, R. Treffeisen, and G. Lohmann, 2019: September Arctic sea ice minimum prediction—A skillful new statistical approach. *Earth Syst. Dyn.*, **10**, 189–203, https://doi.org/10.5194/esd-10-189-2019.

Katlein, C., S. Arndt, H. J. Belter, G. Castellani, and M. Nicolaus, 2019: Seasonal evolution of light transmission distributions through Arctic sea ice. *J. Geophys. Res. Oceans*, **124**, 5418–5435, https://doi.org/10.1029/2018JC014833.

Kim, K.-Y., B. D. Hamlington, H. Na, and J. Kim, 2016: Mechanism of seasonal Arctic sea ice evolution and Arctic amplification. *Cryosphere*, **10**, 2191–2202, https://doi.org/10.5194/tc-10-2191-2016.

Kim, Y. J., H.-C. Kim, D. Han, S. Lee, and J. Im, 2020: Prediction of monthly Arctic sea ice concentrations using satellite and reanalysis data based on convolutional neural networks. *Cryosphere*, **14**, 1083–1104, https://doi.org/10.5194/tc-14-1083-2020.

Kwok, R., 2018: Arctic sea ice thickness, volume, and multiyear ice coverage: Losses and coupled variability (1958–2018). *Environ. Res. Lett.*, **13**, 105005, https://doi.org/10.1088/1748-9326/aae3ec.

Labe, Z., Y. Peings, and G. Magnusdottir, 2018: Contributions of ice thickness to the atmospheric response from projected Arctic sea ice loss. *Geophys. Res. Lett.*, **45**, 5635–5642, https://doi.org/10.1029/2018GL078158.

Landy, J. C., and Coauthors, 2022: A year-round satellite sea-ice thickness record from CryoSat-2. *Nature*, **609**, 517–522, https://doi.org/10.1038/s41586-022-05058-5.

Laxon, S. W., and Coauthors, 2013: CryoSat-2 estimates of Arctic sea ice thickness and volume. *Geophys. Res. Lett.*, **40**, 732–737, https://doi.org/10.1002/grl.50193.

Lee, J., M.-I. Lee, and J.-B. Ahn, 2022: Importance of ocean initial conditions of late autumn on winter seasonal prediction skill in atmosphere–land–ocean–sea ice coupled forecast system. *Climate Dyn.*, **58**, 3427–3440, https://doi.org/10.1007/s00382-021-06106-y.

Lee, S.-W., and J.-M. Song, 2014: Economic possibilities of shipping though northern sea route. *Asian J. Shipp. Logist.*, **30**, 415–430, https://doi.org/10.1016/j.ajsl.2014.12.009.

Lenetsky, J. E., B. Tremblay, C. Brunette, and G. Meneghello, 2021: Subseasonal predictability of Arctic Ocean sea ice conditions: Bering Strait and Ekman-driven ocean heat transport. *J. Climate*, **34**, 4449–4462, https://doi.org/10.1175/JCLI-D-20-0544.1.

Leppäranta, M., V. P. Meleshko, P. Uotila, and T. Pavlova, 2020: Sea ice modelling. *Sea Ice in the Arctic: Past, Present and Future*, O. M. Johannessen et al., Eds., Springer, 315–387, https://doi.org/10.1007/978-3-030-21301-5_8.

Lindsay, R., and A. Schweiger, 2015: Arctic sea ice thickness loss determined using subsurface, aircraft, and satellite observations. *Cryosphere*, **9**, 269–283, https://doi.org/10.5194/tc-9-269-2015.

Lindsay, R. W., J. Zhang, A. J. Schweiger, and M. A. Steele, 2008: Seasonal predictions of ice extent in the Arctic Ocean. *J. Geophys. Res.*, **113**, C02023, https://doi.org/10.1029/2007JC004259.

Liu, J., and Coauthors, 2019: Towards reliable Arctic sea ice prediction using multivariate data assimilation. *Sci. Bull.*, **64**, 63–72, https://doi.org/10.1016/j.scib.2018.11.018.

Liu, Y., L. Bogaardt, J. Attema, and W. Hazeleger, 2021: Extended-range Arctic sea ice forecast with convolutional long short-term memory networks. *Mon. Wea. Rev.*, **149**, 1673–1693, https://doi.org/10.1175/MWR-D-20-0113.1.

Mahoney, A. R., J. K. Hutchings, H. Eicken, and C. Haas, 2019: Changes in the thickness and circulation of multiyear ice in the Beaufort Gyre determined from pseudo-Lagrangian methods from 2003–2015. *J. Geophys. Res. Oceans*, **124**, 5618–5633, https://doi.org/10.1029/2018JC014911.

Meier, W. N., and Coauthors, 2021: Sea ice. NOAA Tech. Rep. OAR ARC 21-05, 9 pp., https://repository.library.noaa.gov/view/noaa/34474.

Meleshko, V. P., V. M. Kattsov, V. M. Mirvis, A. V. Baidin, T. V. Pavlova, and V. A. Govorkova, 2018: Is there a link between Arctic sea ice loss and increasing frequency of extremely cold winters in Eurasia and North America? Synthesis of current research. *Russ. Meteor. Hydrol.*, **43**, 743–755, https://doi.org/10.3103/S1068373918110055.

Msadek, R., G. A. Vecchi, M. Winton, and R. G. Gudgel, 2014: Importance of initial conditions in seasonal predictions of Arctic sea ice extent. *Geophys. Res. Lett.*, **41**, 5208–5215, https://doi.org/10.1002/2014GL060799.

Mu, L., M. Losch, Q. Yang, R. Ricker, S. N. Losa, and L. Nerger, 2018: Arctic-wide sea ice thickness estimates from combining satellite remote sensing data and a dynamic ice-ocean model with data assimilation during the CryoSat-2 period. *J. Geophys. Res. Oceans*, **123**, 7763–7780, https://doi.org/10.1029/2018JC014316.

Notz, D., and J. Stroeve, 2016: Observed Arctic sea-ice loss directly follows anthropogenic CO_2 emission. *Science*, **354**, 747–750, https://doi.org/10.1126/science.aag2345.

——, and SIMIP Community, 2020: Arctic sea ice in CMIP6. *Geophys. Res. Lett.*, **47**, e2019GL086749, https://doi.org/10.1029/2019GL086749.

Peterson, A. K., I. Fer, M. G. McPhee, and A. Randelhoff, 2017: Turbulent heat and momentum fluxes in the upper ocean under Arctic sea ice. *J. Geophys. Res. Oceans*, **122**, 1439–1456, https://doi.org/10.1002/2016JC012283.

Peterson, K. A., A. Arribas, H. T. Hewitt, A. B. Keen, D. J. Lea, and A. J. McLaren, 2015: Assessing the forecast skill of Arctic sea ice extent in the GloSea4 seasonal prediction system. *Climate Dyn.*, **44**, 147–162, https://doi.org/10.1007/s00382-014-2190-9.

Petty, A. A., 2018: A possible link between winter Arctic sea ice decline and a collapse of the Beaufort high? *Geophys. Res. Lett.*, **45**, 2879–2882, https://doi.org/10.1002/2018GL077704.

——, J. K. Hutchings, J. A. Richter-Menge, and M. A. Tschudi, 2016: Sea ice circulation around the Beaufort Gyre: The changing role of wind forcing and the sea ice state. *J. Geophys. Res. Oceans*, **121**, 3278–3296, https://doi.org/10.1002/2015JC010903.

Pithan, F., and T. Mauritsen, 2014: Arctic amplification dominated by temperature feedbacks in contemporary climate models. *Nat. Geosci.*, **7**, 181–184, https://doi.org/10.1038/ngeo2071.

Ponsoni, L., F. Massonnet, T. Fichefet, M. Chevallier, and D. Docquier, 2019: On the timescales and length scales of the Arctic sea ice thickness anomalies: A study based on 14 reanalyses. *Cryosphere*, **13**, 521–543, https://doi.org/10.5194/tc-13-521-2019.

——, ——, D. Docquier, G. Van Achter, and T. Fichefet, 2020: Statistical predictability of the Arctic sea ice volume anomaly: Identifying predictors and optimal sampling locations. *Cryosphere*, **14**, 2409–2428, https://doi.org/10.5194/tc-14-2409-2020.

Ren, Y., X. Li, and W. Zhang, 2022: A data-driven deep learning model for weekly sea ice concentration prediction of the Pan-Arctic during the melting season. *IEEE Trans. Geosci. Remote Sens.*, **60**, 1–19, https://doi.org/10.1109/TGRS.2022.3177600.

Ricker, R., S. Hendricks, L. Kaleschke, X. Tian-Kunze, and C. Haas, 2017: A weekly Arctic sea-ice thickness data record from merged CryoSat-2 and SMOS satellite data. *Cryosphere*, **11**, 1607–1623, https://doi.org/10.5194/tc-11-1607-2017.

Schweiger, A., R. Lindsay, J. Zhang, M. Steele, H. Stern, and R. Kwok, 2011: Uncertainty in modeled Arctic sea ice volume. *J. Geophys. Res.*, **116**, C00D06, https://doi.org/10.1029/2011JC007084.

Screen, J. A., and I. Simmonds, 2010: The central role of diminishing sea ice in recent Arctic temperature amplification. *Nature*, **464**, 1334–1337, https://doi.org/10.1038/nature09051.

——, and J. A. Francis, 2016: Contribution of sea-ice loss to Arctic amplification is regulated by Pacific Ocean decadal variability. *Nat. Climate Change*, **6**, 856–860, https://doi.org/10.1038/nclimate3011.

Segal, R. A., R. K. Scharien, F. Duerden, and C.-L. Tam, 2020: The best of both worlds: Connecting remote sensing and Arctic communities for safe sea ice travel. *Arctic*, **73**, 405–550, https://doi.org/10.14430/arctic71896.

Semenova, T., 2022: Value improving practices in production of hydrocarbon resources in the Arctic regions. *J. Mar. Sci. Eng.*, **10**, 187, https://doi.org/10.3390/jmse10020187.

Sévellec, F., A. V. Fedorov, and W. Liu, 2017: Arctic sea-ice decline weakens the Atlantic meridional overturning circulation. *Nat. Climate Change*, **7**, 604–610, https://doi.org/10.1038/nclimate3353.

Shamshiri, R., E. Eide, and K. V. Hoyland, 2022: Spatio-temporal distribution of sea-ice thickness using a machine learning approach with Google Earth Engine and Sentinel-1 GRD data. *Remote Sens. Environ.*, **270**, 112851, https://doi.org/10.1016/j.rse.2021.112851.

Smith, D. M., N. J. Dunstone, A. A. Scaife, E. K. Fiedler, D. Copsey, and S. C. Hardiman, 2017: Atmospheric response to Arctic and Antarctic sea ice: The importance of ocean–atmosphere coupling and the background state. *J. Climate*, **30**, 4547–4565, https://doi.org/10.1175/JCLI-D-16-0564.1.

Stroeve, J. C., A. D. Crawford, and S. Stammerjohn, 2016: Using timing of ice retreat to predict timing of fall freeze-up in the Arctic. *Geophys. Res. Lett.*, **43**, 6332–6340, https://doi.org/10.1002/2016GL069314.

Suo, L., Y. Gao, D. Guo, and I. Bethke, 2017: Sea-ice free Arctic contributes to the projected warming minimum in the North Atlantic. *Environ. Res. Lett.*, **12**, 074004, https://doi.org/10.1088/1748-9326/aa6a5e.

Thorndike, A. S., D. A. Rothrock, G. A. Maykut, and R. Colony, 1975: The thickness distribution of sea ice. *J. Geophys. Res.*, **80**, 4501–4513, https://doi.org/10.1029/JC080i033p04501.

Tietsche, S., and Coauthors, 2014: Seasonal to interannual Arctic sea ice predictability in current global climate models. *Geophys. Res. Lett.*, **41**, 1035–1043, https://doi.org/10.1002/2013GL058755.

Tschudi, M. A., J. C. Stroeve, and J. S. Stewart, 2016: Relating the age of Arctic sea ice to its thickness, as measured during NASA's ICESat and IceBridge campaigns. *Remote Sens.*, **8**, 457, https://doi.org/10.3390/rs8060457.

Wang, L., X. Yuan, M. Ting, and C. Li, 2016: Predicting summer Arctic sea ice concentration intraseasonal variability using a vector autoregressive model. *J. Climate*, **29**, 1529–1543, https://doi.org/10.1175/JCLI-D-15-0313.1.

——, ——, and C. Li, 2019: Subseasonal forecast of Arctic sea ice concentration via statistical approaches. *Climate Dyn.*, **52**, 4953–4971, https://doi.org/10.1007/s00382-018-4426-6.

Wang, X., J. Key, R. Kwok, and J. Zhang, 2016: Comparison of Arctic sea ice thickness from satellites, aircraft, and PIOMAS data. *Remote Sens.*, **8**, 713, https://doi.org/10.3390/rs8090713.

——, Y. Liu, J. R. Key, and R. Dworak, 2022: A new perspective on four decades of changes in Arctic sea ice from satellite

observations. *Remote Sens.*, **14**, 1846, https://doi.org/10.3390/rs14081846.

Wang, Y., H. Bi, H. Huang, Y. Liu, Y. Liu, X. Liang, M. Fu, and Z. Zhang, 2019a: Satellite-observed trends in the Arctic sea ice concentration for the period 1979–2016. *J. Oceanol. Limnol.*, **37**, 18–37, https://doi.org/10.1007/s00343-019-7284-0.

——, X. Yuan, H. Bi, Y. Liang, H. Huang, Z. Zhang, and Y. Liu, 2019b: The contributions of winter cloud anomalies in 2011 to the summer sea-ice rebound in 2012 in the Antarctic. *J. Geophys. Res. Atmos.*, **124**, 3435–3447, https://doi.org/10.1029/2018JD029435.

——, ——, ——, M. Bushuk, Y. Liang, C. Li, and H. Huang, 2022a: Reassessing seasonal sea ice predictability of the Pacific-Arctic sector using a Markov model. *Cryosphere*, **16**, 1141–1156, https://doi.org/10.5194/tc-16-1141-2022.

——, ——, and M. A. Cane, 2022b: Coupled mode of cloud, atmospheric circulation, and sea ice controlled by wave-3 pattern in Antarctic winter. *Environ. Res. Lett.*, **17**, 044053, https://doi.org/10.1088/1748-9326/ac5272.

Wayand, N. E., C. M. Bitz, and E. Blanchard-Wrigglesworth, 2019: A year-round subseasonal-to-seasonal sea ice prediction portal. *Geophys. Res. Lett.*, **46**, 3298–3307, https://doi.org/10.1029/2018GL081565.

Yang, C.-Y., J. Liu, and D. Chen, 2022: An improved regional coupled modeling system for Arctic sea ice simulation and prediction: A case study for 2018. *Geosci. Model Dev.*, **15**, 1155–1176, https://doi.org/10.5194/gmd-15-1155-2022.

Yang, Q., T. H. Dixon, P. G. Myers, J. Bonin, D. Chambers, M. R. van den Broeke, M. H. Ribergaard, and J. Mortensen, 2016: Recent increases in Arctic freshwater flux affects Labrador Sea convection and Atlantic overturning circulation. *Nat. Commun.*, **7**, 13545, https://doi.org/10.1038/ncomms13545.

Yuan, X., D. Chen, C. Li, L. Wang, and W. Wang, 2016: Arctic sea ice seasonal prediction by a linear Markov model. *J. Climate*, **29**, 8151–8173, https://doi.org/10.1175/JCLI-D-15-0858.1.

Zhang, J., and D. Rothrock, 2001: A thickness and enthalpy distribution sea-ice model. *J. Phys. Oceanogr.*, **31**, 2986–3001, https://doi.org/10.1175/1520-0485(2001)031<2986:ATAEDS>2.0.CO;2.

——, and D. A. Rothrock, 2003: Modeling global sea ice with a thickness and enthalpy distribution model in generalized curvilinear coordinates. *Mon. Wea. Rev.*, **131**, 845–861, https://doi.org/10.1175/1520-0493(2003)131<0845:MGSIWA>2.0.CO;2.

Zhou, X., C. Min, Y. Yang, J. C. Landy, L. Mu, and Q. Yang, 2021: Revisiting trans-Arctic maritime navigability in 2011–2016 from the perspective of sea ice thickness. *Remote Sens.*, **13**, 2766, https://doi.org/10.3390/rs13142766.

Zuo, H., M. A. Balmaseda, S. Tietsche, K. Mogensen, and M. Mayer, 2019: The ECMWF operational ensemble reanalysis-analysis system for ocean and sea ice: A description of the system and assessment. *Ocean Sci.*, **15**, 779–808, https://doi.org/10.5194/os-15-779-2019.